

Paleoceanography and Paleoclimatology*

RESEARCH ARTICLE

10.1029/2022PA004486

Key Points:

- Volume transport through the Tsushima Strait reduces non-linearly when the sea level reduces linearly
- Sea surface salinity of the Japan Sea reached its minimum value (20.2) at 20 kyr BP
- Volume transport through the Tsushima Strait dominates the value and timing of the minimum salinity, and $P-E$ can modify the former

Supporting Information:

Supporting Information may be found in the online version of this article.

Correspondence to:

X. Guo,
guoxinyu@sci.ehime-u.ac.jp


Citation:

Zheng, J., Guo, X., Yang, H., Du, K., Mao, X., Jiang, W., et al. (2023). Low sea surface salinity event of the Japan Sea during the Last Glacial Maximum. *Paleoceanography and Paleoclimatology*, 38, e2022PA004486. <https://doi.org/10.1029/2022PA004486>

Received 24 MAY 2022

Accepted 26 DEC 2022

Low Sea Surface Salinity Event of the Japan Sea During the Last Glacial Maximum

Junyong Zheng^{1,2,3} , Xinyu Guo^{3,4} , Haiyan Yang⁵, Kailun Du⁶, Xinyan Mao^{1,2} , Wensheng Jiang⁶ , Takuya Sagawa⁷ , Yasumasa Miyazawa⁴ , Sergey M. Varlamov⁴, Ayako Abe-Ouchi⁸ , and Wing-Le Chan^{8,9} 

¹Key Laboratory of Physical Oceanography, Ministry of Education, Ocean University of China, Qingdao, China, ²College of Oceanic and Atmospheric Sciences, Ocean University of China, Qingdao, China, ³Center for Marine Environmental Studies, Ehime University, Matsuyama, Japan, ⁴Application Laboratory, Japan Agency for Marine-Earth Science and Technology, Yokohama, Japan, ⁵Graduate School of Science and Engineering, Ehime University, Matsuyama, Japan, ⁶Key Laboratory of Marine Environment and Ecology, Ministry of Education, Ocean University of China, Qingdao, China, ⁷Institute of Science and Engineering, Kanazawa University, Kanazawa, Japan, ⁸Atmosphere and Ocean Research Institute, University of Tokyo, Tokyo, Japan, ⁹Now at Research Center for Environmental Modeling and Application, Japan Agency for Marine-Earth Science and Technology, Yokohama, Japan

Abstract Abnormal lightening of the oxygen isotope ratio ($\delta^{18}\text{O}$) of planktonic foraminifera during the Last Glacial Maximum (LGM, ~ 21 kyr BP) suggests that the Japan Sea had experienced a low sea surface salinity event at that time. However, the exact value and timing of minimum salinity have been controversial so far. To address this issue, we adopt a simple box model and reconstruct the sea surface salinity in the Japan Sea (S_{JP}) over the past 35 kyr with a focus on the LGM period. In particular, as input data for the box model, the inflow transport through the Tsushima Strait (Q) is converted from sea level evolution using a newly defined relationship, in which Q reduces non-linearly with the sea level reduction through a dynamically-constrained realistic ocean model. Meanwhile, another input data of the box model, sea surface freshwater flux (precipitation minus evaporation ($P-E$) evolution), is obtained by averaging multi-paleoclimate models (PMIP3 and MIROC4m models) results. The reconstructed S_{JP} using the box model reached its minimum value (20.2) at 20 kyr BP with a high coefficient of determination (R^2) for $\delta^{18}\text{O}$ (0.81, $p \ll 0.01$). Further analysis demonstrates that the above non-linear relationship, determined by $h^{3/2}$ (h is the strait depth), promises a more reasonable reconstruction of the S_{JP} evolution. It is also concluded that both the value and timing of the minimum S_{JP} depend on the Q evolution, and the $P-E$ evolution can modify the former. Therefore, the combination of Q and $P-E$ determines the exact value and timing of minimum salinity.

Plain Language Summary Twenty one thousand years ago, as a large volume of water froze over land at the Last Glacial Maximum (LGM), the global sea level was depressed by about 130 m. Some semi-enclosed marginal seas with shallow entrances, like the Japan Sea, became completely or almost isolated. Limited communication with the surrounding seas and continuous freshwater input led to a low surface salinity event in the Japan Sea. With two refinements on prior reconstructions of surface salinity, we configure a simple box model to obtain its minimum value (20.2) at 20 kyr BP. Among two refinements, one is a nonlinear-constrained evolution of the inflow transport through the Tsushima Strait; the other is a more reasonable evolution of freshwater flux from multi-paleoclimate models. The reduction of surface salinity could enhance the density stratification and severely restrict the deep convection, leaving a poorly-ventilated, anoxic, and sulfidic deep water, which has been suggested for the environment in the Japan Sea during the LGM. It is noted that such box models can be applied to other semi-enclosed marginal seas.

1. Introduction

The Last Glacial Maximum (LGM, ~ 21 kyr BP) is the most recent interval marked by a maximum expansion of continental ice sheets associated with a global sea level lowstand (Clark et al., 2009; Spötl et al., 2021). It has been suggested that the sea level was ~ 130 m lower during the LGM than at present (e.g., Fairbanks, 1989; Gowan et al., 2021; Stiller et al., 2021; Yokoyama & Purcell, 2021; Yokoyama et al., 2000, 2019). With a decrease in sea level of ~ 130 m, it is easy to imagine that many shallow shelf seas or bays at present were land during the

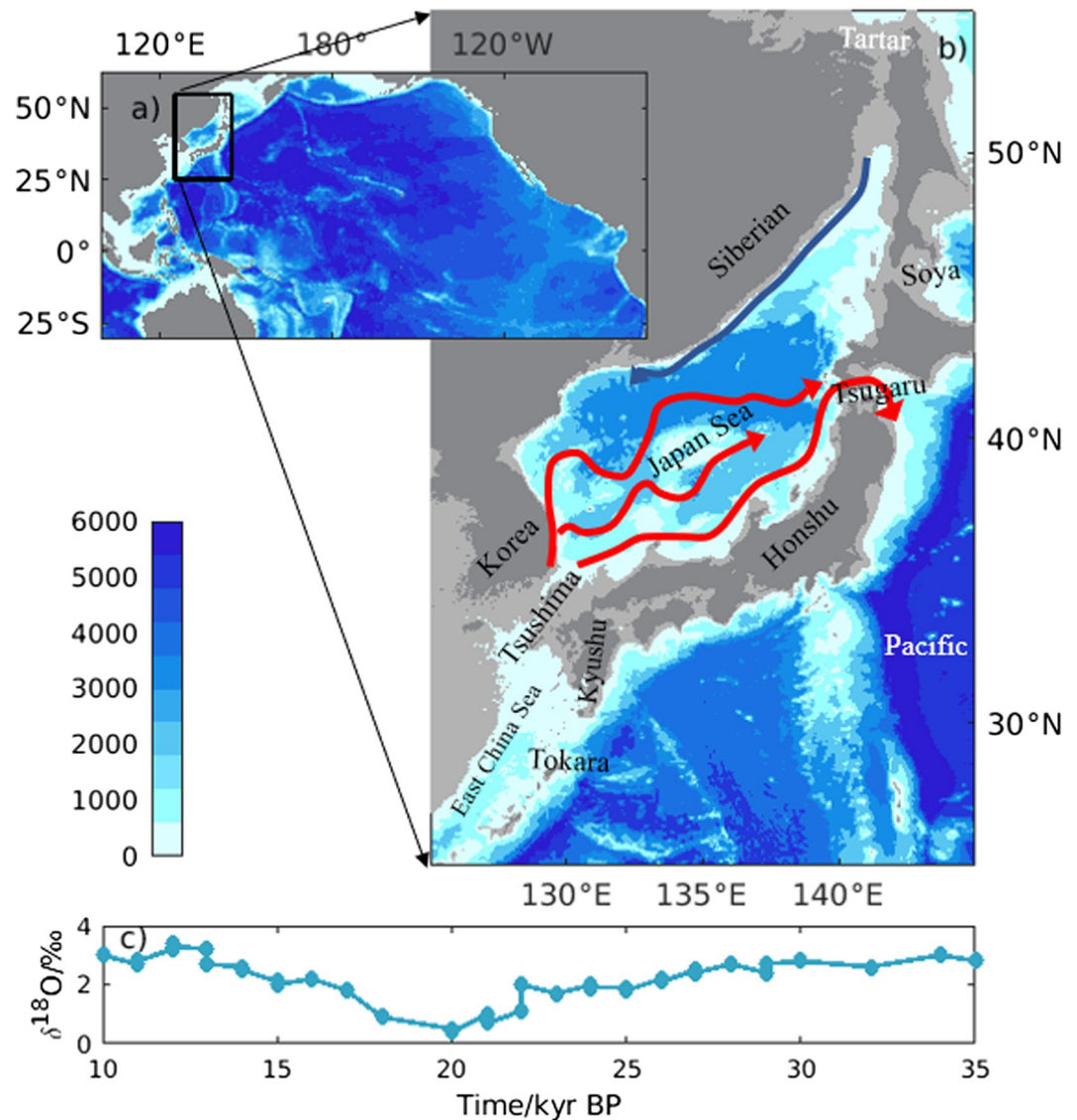


Figure 1. (a) Model domain of the realistic numerical model and its bathymetry (unit: m) under the present sea level (0 m). (b) Enlarged view of the black box in (a) around the Japan Sea area. Light and dense gray areas indicate land under Last Glacial Maximum (-130 m) and present sea level, respectively. Red arrows indicate three branches of the Tsushima Warm current (the East Korea Warm Branch, Offshore Branch, and Nearshore Branch from west to east). Blue arrow indicates the Liman Cold Current. (c) Evolution of oxygen isotopic ratio ($\delta^{18}O$) in planktonic foraminifera adapted from Sagawa et al. (2018).

LGM. Some semi-enclosed marginal seas or fjords with shallow entrances have become completely or almost isolated (E. Lee, Kim, & Nam, 2008).

A typical example is the Japan Sea in the Northwest Pacific (Figures 1a and 1b). The Japan Sea is a deep ($\sim 1,500$ m in depth) but semi-enclosed marginal sea surrounded by the Eurasian Continent and Japanese Archipelago (Kida et al., 2016). It is connected with the surrounding seas through four shallow and narrow straits: the Tsushima Strait (~ 130 m) connecting to the East China Sea, the Tsugaru Strait (~ 130 m) to the Northwest Pacific, and the Soya and Tartar Straits (~ 55 and ~ 12 m, respectively) to the Sea of Okhotsk (E. Lee, Kim, & Nam, 2008; Oba & Irino, 2012). With present-day sea level (dense gray area in Figure 1b), the water exchange between the Japan Sea and surrounding seas involves warmer and saltier inflow through the Tsushima Strait (2.64 Sv, Shin et al., 2022, $1 \text{ Sv} \equiv 10^6 \text{ m}^3 \text{ s}^{-1}$), and colder and fresher outflow through the Tsugaru and Soya Straits (1.5 and 0.91 Sv, respectively, Japan Sea Throughflows). Transport through the Tartar Strait (< 0.05 Sv) is

negligible compared to transport through the other straits (Tsujino et al., 2008; Yanagi, 2002). The upper 200-m layer of the Japan Sea, which is above the permanent pycnocline, is profoundly affected by the throughflows (Isobe, 2020; Oba & Irino, 2012; Yanagi, 2002). Coupled with the air-sea heat flux and freshwater input, the throughflows maintain the heat and salinity budget balance of the upper Japan Sea (Dong et al., 2020; Kida et al., 2016; Wu et al., 2020). As partial original water source, the inflow through the Tsushima Strait was also suggested to contribute to the formations of the intermediate and deep water masses (Gamo et al., 2014; S. Kim et al., 2021; J. Park & Lim, 2018). With a decrease in sea level of ~130 m, shelves of these four straits were exposed and the Japan Sea was either completely or almost isolated from adjacent seas during the LGM (light gray area in Figure 1b; Isobe, 2020; Oba & Irino, 2012; Wu et al., 2020; Yokoyama et al., 2007). Water exchange with the throughflows was extremely limited and drastic regulation of oceanographic conditions naturally occurred in the upper Japan Sea (E. Lee & Nam, 2004). In this study, we focus on the influence of this isolation event on the surface salinity in the Japan Sea (S_{jp}).

The recovery of this drastic regulation event of S_{jp} during the LGM has been diligently examined in many studies (K. E. Lee, 2007; Sagawa et al., 2018; Wu et al., 2020). The oxygen isotope ratio ($\delta^{18}\text{O}$) of planktonic foraminifera in the sediments, as a recorder of paleoenvironmental conditions in the Japan Sea, could faithfully explain this regulation story. It has been suggested that $\delta^{18}\text{O}$ ratio experienced a sharp reduction from ~30 kyr BP, with a minimum value around the LGM (Figure 1c; Matsui et al., 1998; Oba et al., 1991; Sagawa et al., 2018; Wu et al., 2020; Yokoyama et al., 2007). A minimum $\delta^{18}\text{O}$ generally corresponds to highest temperature or lowest salinity at the sea surface (Ravelo & Hillaire-Marcel, 2007; Yokoyama et al., 2007).

Over the past several decades, the alkenone thermometry has been applied to reconstruct sea surface temperature (SST) of the Japan Sea. Ishiwatari et al. (2001) reported a high alkenone-based ($U_{37}^{K'}$) SST as 18°C–19°C during the LGM, 2°C–3°C higher than that during Holocene, which was probably caused by thermal energy of solar radiation trapped in the stable stratified surface seawater. This high SST was also identified by Fujine et al. (2009), Liu et al. (2014), and Wu et al. (2020). However, unusually high $U_{37}^{K'}$ -SSTs was not found in K. E. Lee, Bahk, and Choi (2008) and Y. H. Park and Khim (2022). Yokoyama et al. (2007) suggested that the alkenone content was dramatically low during the LGM, and thus difficult to calculate $U_{37}^{K'}$ -SST. Fujine et al. (2009) further indicated that low salinity may have an ecological or physiological influence on the alkenone proxy, and thereby regarded the high SST as anomalous. Furthermore, the warm LGM SST was not supported by micropaleontological studies (Yokoyama et al., 2007). Records from diatom, benthic and planktonic foraminifera, and radiolarian species revealed that SST during the LGM was much lower than that of today (Hyun et al., 2013; Itaki et al., 2007; Koizumi & Yamamoto, 2011; Matsui et al., 1998; Nakagawa et al., 2003; Oba & Tanimura, 2012). Although the SST of the Japan Sea during the LGM remains controversial, we assumed that, supported by the above descriptions, the SST during the LGM was not higher than that in other periods. Following this assumption, the abnormal reduction in $\delta^{18}\text{O}$ there strongly suggests a low S_{jp} event (S. Gorbarenko et al., 2021; E. Lee, Kim, & Nam, 2008; Matsui et al., 1998). However, partly because of the unclear relationship between $\delta^{18}\text{O}$ and S_{jp} , previous studies leave the exact value of minimum S_{jp} during the LGM as disputable (28, Oba et al., 1991; 20, Tada, 1999; 29.8, S. A. Gorbarenko & Southon, 2000; 26–29, Oba & Tanimura, 2012).

The box model, based on water and salinity budget balance in the Japan Sea, has been employed to resolve this controversy. Matsui et al. (1998) adopted a salinity-balance box model for the upper Japan Sea to reconstruct S_{jp} evolution over the past 35 kyr. They obtained a minimum S_{jp} of 20 during 20–15 kyr BP. Similarly, Ikeda et al. (1999) employed two boxes to represent the northern and southern parts of the upper 300 m in the Japan Sea, and estimated that the S_{jp} in the two boxes reached their minimum values (28.83, 29.59) during 17–15 kyr BP. Despite the minimum S_{jp} (value and timing) differences, the box model provides an alternative and feasible method to quantify low-salinity event.

The calculated minimum S_{jp} depends strongly on the inflow transport through the Tsushima Strait (Q) and the precipitation minus evaporation ($P-E$) evolution for the box model. However, it is challenging to estimate continuously and precisely through a direct methodology. As a compromise, Matsui et al. (1998) assumed a linear relationship between Q and the Tsushima Strait depth (sea level), and used it to convert the sea level evolution into Q evolution, but without verifying this relationship. Ikeda et al. (1999) simply specified an idealistic Q evolution (linearly decreased from 1.0 to 0.01 Sv between 25 and 17 kyr BP, remained at 0.01 Sv over 17–15 kyr BP, linearly increased to 1.5 Sv from 15 to 10 kyr BP and remained at 1.5 Sv until present day). An idealistic $P-E$ evolution was also specified and remained as a time-independent constant ($0.3 \text{ m y}^{-1} \approx 0.82 \text{ mm d}^{-1}$) both in Matsui

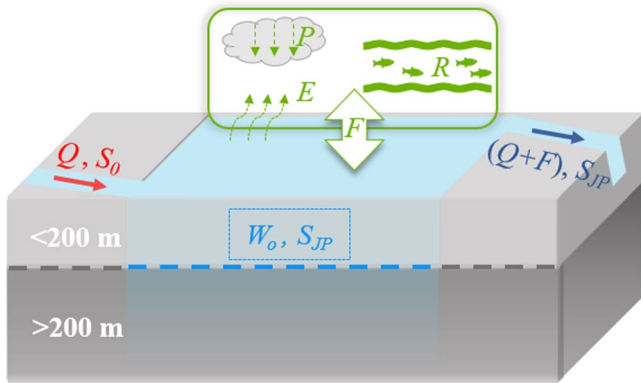


Figure 2. Schematic of the box model for S_{JP} reconstruction. This box model focuses on the upper 200-m Japan Sea and its total volume is defined as W_0 . Water mass conservation is among inflow through the Tsushima Strait Q , freshwater flux F , and outflow through the Tsugaru and Soya Straits $Q + F$. The freshwater flux here comprises precipitation over evaporation $P-E$, and river discharge R . The conservation of salinity is between inflow salinity QS_0 and outflow salinity $(Q + F)S_{JP}$.

et al. (1998) and Ikeda et al. (1999). Apparently, the Q and $P-E$ evolutions used in the above studies are not supported by paleoceanographic evidence nor do they have dynamical constraints, and therefore more careful examinations and refinements for a reasonable S_{JP} reconstruction are needed.

In this study, we also design a box model to reconstruct the S_{JP} evolution over the past 35 kyr with a focus on the low S_{JP} event at the LGM. As an improvement over Matsui et al. (1998) and Ikeda et al. (1999), we refine the Q and $P-E$ evolutions to obtain a more precise value and timing for minimum S_{JP} . For the Q evolution, we will first quantify the relationship between Q and sea level through a basin-scale realistic hydrodynamic model. This realistic model, constrained by dynamical equations, could provide a more reasonable relationship than that assumed by Matsui et al. (1998). Investigation of this relationship is meaningful for the study of regional paleoenvironmental changes around the Japan Sea. More importantly, such an investigation could capture local effects exerted by remote forcing from the open sea during the last deglaciation (Nishida & Ikehara, 2013; Oba et al., 1991). This is because local sea level difference (high in south of the Tsushima Strait and low in east of the Tsugaru and Soya Straits), which dominates the mean value of Q , was remotely controlled by the basin-scale wind stress over the North Pacific (Minato & Kimura, 1980; Ohshima, 1994; Tsujino et al., 2008). Assisted by this dynamically-constrained relationship, the Q evolution can be converted

from sea level evolution provided by previous studies (e.g., Yokoyama et al., 2018). Meanwhile, multi-model simulation results from the third phase of the Paleoclimate Modeling Intercomparison Project (PMIP3) and Model for Interdisciplinary Research on Climate 4m (MIROC4m) are also involved, which offer an excellent opportunity to refine the $P-E$ evolution more comprehensively and quantitatively.

The remainder of this paper is organized as follows. Details of the box model and methods used to refine the Q and $P-E$ evolutions are introduced in Section 2. Section 3 shows the relation between the Q and sea level and the Q , $P-E$, and reconstructed S_{JP} evolutions over the past 35 kyr. Section 4 includes further discussions and Section 5 presents the summary.

2. Materials and Methods

A simple box model for S_{JP} reconstruction is laid out in this section. Methods to refine its input data (Q and $P-E$ evolutions) are given in detail.

2.1. Box Model

Similar to previous studies (e.g., Matsui et al., 1998; Topper et al., 2011), conservation of water mass and balance of salt budget provide the framework for this box model. In this model, the following four points are considered. (a) Only the upper 200 m of the Japan Sea is considered in this box model and its total volume W_0 is assumed as a constant ($1.5 \times 10^{14} \text{ m}^3$, Yanagi, 2002). A sensitivity experiment and analysis in the Text S1 in Supporting Information S1 suggest the acceptability of this assumption; (b) Freshwater flux (F), inflow, and outflow through straits are taken into consideration, while the vertical water exchange between the upper 200 m and the layer below is neglected. F here contains $P-E$ and river discharge (R); (c) Response of S_{JP} to external influences mentioned above is instantaneous, that is, the box is always well mixed; and (d) The salinity of adjacent seas around the Japan Sea does not change over time. Based on these considerations, we establish a salt-balance box model (Figure 2), which can be formulated as:

$$\frac{dS_{JP}(t)}{dt} = \frac{Q(t)S_0 - [Q(t) + F(t)]S_{JP}(t)}{W_0} \quad (1)$$

$$F(t) = P(t) - E(t) + R(t) \quad (2)$$

The meanings of each symbol in these two equations are listed in Table 1. The salt input through the Tsushima Strait is calculated by multiplying its volume transport $Q(t)$ with salinity S_0 , that is, $Q(t)S_0$. Correspondingly, salt output through the Tsugaru and Soya Straits is $[Q(t) + F(t)]S_{JP}(t)$. The salt through the Tartar Strait is negligible

Table 1
Variables and Parameters Related to the Box Model

Variable or parameter	Meaning	Method or value	Reference
$Q(t)$	Inflow transport	This study	–
$P(t)$	Precipitation over Japan Sea	PMIP3, MIROC4m	–
$E(t)$	Evaporation over Japan Sea	PMIP3, MIROC4m	–
$F(t)$	Freshwater flux	$P(t)-E(t) + R$	Yanagi (2002)
$R(t)$	River discharge	Linearly proportional to $P(t)$	–
S_0	Inflow salinity	33	Matsui et al. (1998)
W_0	Volume of upper Japan Sea	$1.5 \times 10^{14} \text{ m}^3$	Yanagi (2002)
$S_{JP}(t)$	Salinity of upper Japan Sea	To be resolved	–

because its volume transport is much smaller than that through the other three straits, as described in the Introduction. The difference between salt input and output for the upper 200 m of the Japan Sea (W_0) determines the evolution of $S_{JP}(t)$. The calculation method and value of input variables and parameters in the two equations are also presented in Table 1, where unknown variables are marked in bold. Notably, we assume that $R(t)$ is linearly proportional to $P(t)$ as $R(t) = \alpha P(t)$, where α is a constant coefficient calculated as the ratio of river discharge and precipitation rate under present day. With the specified Q and $P-E$ evolutions, the temporal variation of S_{JP} during the evolution period can be calculated using Equation 1. Methods to determine Q and $P-E$ evolutions are introduced in the following section.

2.2. Methods to Refine the Q and $P-E$ Evolutions

2.2.1. Refinement to the Q Evolution

As a first step, we introduce and develop a basin-scale realistic numerical model to examine the relationship between Q and sea level. Second, sea level evolution from previous studies is also described. Under this newly defined relationship, sea level evolution can be converted into Q evolution.

2.2.1.1. Experiments Using the Realistic Numerical Model

A basin-scale numerical model incorporating realistic bathymetry and meteorological forcing (wind stresses, heat fluxes, and salt fluxes) over the North Pacific and Japan Sea is involved here. The source codes come from the Stony Brook Parallel Ocean Model (sbPOM, Jordi & Wang, 2012). The model domain covers the entire North Pacific and the Japan Sea (30°S–62°N, 100°E–70°W, Figure 1a) with a horizontal resolution of 1/4° and 21 terrain-following vertical layers. Detailed configurations of this realistic numerical model could be found in the Text S2 in Supporting Information S1.

The calculation for realistic model (R-CTRL) is set under the present sea level (0 m) and the model is evaluated by judging whether it can capture the basic features of the annual mean Q . To reveal the regression relationship between the Q and sea level, 13 sensitivity experiments (R-SENS) are conducted by modifying the sea level in R-CTRL. In these experiments (R-SENS), the sea level decreases linearly from 0 m to –130 m at intervals 10 m. This is the only change from the R-CTRL. After fixing the new water depth of each grid point in R-SENS, the initial and boundary conditions for R-SENS are obtained in the same way as R-CTRL. All the experiments are started from an equilibrated ocean and run continuously for 40 years. We treat the first 35 years as the spin-up phase and use the annual mean model results from the final 5 years for analysis.

2.2.1.2. Sea Level Evolution

Apart from this regression relationship derived from the realistic model, another variable for refining the Q evolution is the change in global mean sea level, which is adapted from Yokoyama et al. (2018; Figure 3a). The sea level change was derived from fossil coral reef material obtained from the Great Barrier Reef in Australia during the Integrated Ocean Drilling Program (IODP) Expedition 325, combined with data through glacio-isostatic modeling. Figure 3a shows a rapid fall (~45 m) in sea level from 32 to 29 kyr BP after an initial gentle fall (~5 m) from 35 to 32 kyr BP. A relatively constant sea level was construed at 28–22 kyr BP. Subsequently, the sea level reached its lowest value (<–125 m) within a short period (~2 kyr) around 20 kyr BP. From then on, the sea level

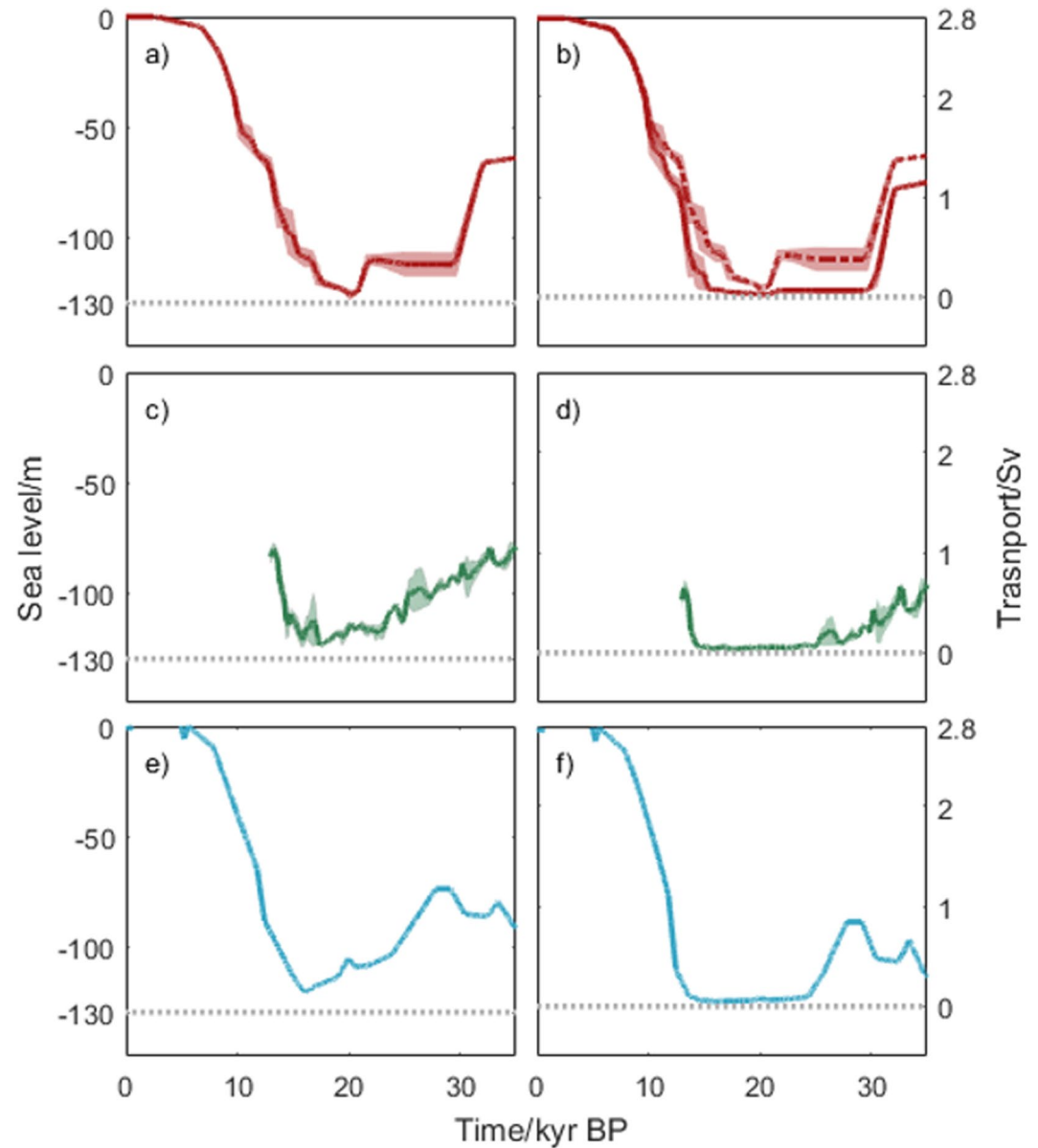


Figure 3. The sea level and Q evolutions. Solid lines in (a), (c), and (e) represent the sea level evolutions adapted from Yokoyama et al. (2018), Arz et al. (2007), and Saito et al. (1998), respectively. The solid lines in (b), (d), and (f) are Q evolutions derived from (a), (c), and (e) under the non-linear regression relationship, respectively. The dashed line in (b) is the same as the solid one but under the linear regression relationship. Width of the curves represents analytical uncertainties from sea level. The dotted lines denote the sea level at -130 m for (a), (c), and (e), and transport at zero for (b), (d), and (f).

exhibited an increasing trend until present with several rapid melting events. The width of the curve in Figure 3a represents the analytical uncertainties at the sea level.

To explore the influence of Q evolution on S_{JP} reconstruction, especially on the value and timing of minimum S_{JP} , the sea level changes reported by Arz et al. (2007) and Saito et al. (1998) are also used to calculate the Q evolutions for the box model. These two kinds of sea level evolutions (Figures 3c and 3e) were reproduced from benthic $\delta^{18}O$ in the northern Red Sea and radiocarbon dating of shells in the East China Sea, respectively. Although detailed features among these three types of sea level evolutions are different, the values of the lowest sea level were all smaller than -120 m and occurred around 20 kyr BP.

Overall, the sea level has gone through a series of changes over the past 35 kyr. A drastic Q evolution is expected and will be obtained with the new regression relationship with the sea level mentioned above.

Table 2
Basic Information About the PMIP3 and MIROC4m Models

Model	Atmosphere resolution (Latitude × Longitude)	Reference
CCSM4	1.25° × ~0.90°	Gent et al. (2011)
CNRM-CM5	~1.40° × ~1.40°	Voldoire et al. (2013)
FGOALS-g2	~2.80° × ~3–6°	L. Li et al. (2013)
IPSL-CM5A-LR	~3.75° × ~1.90°	Dufresne et al. (2013)
MIROC-ESM	~2.80° × ~2.80°	Watanabe et al. (2011)
MPI-ESM-P	~1.87° × ~1.87°	Giorgetta et al. (2013)
MRI-CGCM3	~1.12° × ~1.12°	Yukimoto et al. (2012)
MIROC4m	~2.80° × ~2.80°	Chan et al. (2011)

2.2.2. Refinement to the *P-E* Evolution

We use simulation results from the PMIP3 and MIROC4m models to refine the *P-E* evolution over the past 35 kyr. The PMIP was first established in the early 1990s to provide a framework for coordinating paleoclimate modeling, paleo-data syntheses, and evolution to analyze and understand climate change and its feedbacks (Braconnot et al., 2012; Harrison et al., 2015). The PMIP coordinated experiments, conducted by multiple modeling groups, reproduced features of several key historical periods by imposing suitable changes in the boundary conditions. Detailed information regarding these experiments is provided at <https://esgf-node.ipsl.upmc.fr/search/esgf-ipsl/>. Here, monthly simulation results of the LGM, Mid-Holocene (MH, 6 kyr BP), and Pre-industrial (PI, 0 kyr BP) experiments from the CCSM4, CNRM-CM5, FGOALS-g2, IPSL-CM5A-LR, MIROC-ESM, MPI-ESM-P, and MRI-CGCM3 models within the framework of PMIP3 (Table 2) are used to quantify the *P-E* evolution. Pre-processing is performed on the above results by calculating the temporal mean at these three periods, and averaging

spatially over the Japan Sea area (35°N–52°N, 128°E–142°E). Moreover, MIROC4m simulation results are employed to provide data for these three periods and two extra historical regimes (35 and 30 kyr BP) with the same pre-processing. MIROC4m is a coupled atmosphere-ocean general circulation model, where m stands for mid-resolution (horizontal resolution of the atmospheric model is ~2.8°; Table 2). This model has been widely used to simulate paleoclimatic changes (e.g., Sherriff-Tadano et al., 2021).

The *P-E* evolution is refined by averaging these multi-model simulation results for 35 and 30 kyr BP, LGM, MH, and PI, which is considered to be a means of reducing the uncertainty from each of the models. Additionally, simulation result from each model is also employed to quantify the impact of *P-E* evolution on the minimum S_{jp} .

3. Results

In this section, the regression relationship between Q and sea level is derived from the realistic ocean model result. With this relationship, the sea level evolution over the past 35 kyr is converted to the Q evolution. The box model thereafter is used to demonstrate the S_{jp} evolution and its minimum value with a combination of this Q evolution and the averaged *P-E* evolution.

3.1. Q Evolution

3.1.1. Variations in the Flow Field Around the Japan Sea

Before presenting the regression relationship, it is worth describing mean elevation, and velocity patterns averaged over the final 5 years of the realistic model results to demonstrate how the flow field around the Japan Sea varies with decreasing sea levels. The horizontal distribution of the mean elevation and sea surface velocity around the Japan Sea, simulated by R-CTRL and R-SENS, are shown in Figures 4 and 5, respectively. Among the results from R-SENS, only those with sea level decreasing to –30, –60, –90, and –130 m are provided, which are sufficient to address the response of the flow field to sea level change.

For the mean elevation patterns (Figure 4), the –0.2 m contour line in each pattern is marked as white for a better view. The mean elevation from the R-CTRL simulation is characterized by a decrease from south to north with the –0.2 m contour line in the middle of the Japan Sea (Figure 4a). The highest magnitude (≥ 0.50 m) is located south of the Japanese Archipelago, where the Kuroshio alternates between a straight and meandering path. The lowest magnitude (≤ -0.50 m) is located along the coasts of Siberia and North Korea, where a distinctive current, named the Liman Cold Current, flows southward (Figure 1b). Among the R-SENS patterns (Figures 4b–4e), one of the most evident features, compared with R-CTRL, is that the elevation inside the Japan Sea tends to decrease as the sea level decreases. The –0.2 m contour line moves southward gradually and out of the Japan Sea when the sea level is at –90 and –130 m (Figures 4d and 4e).

The mean sea surface velocity patterns for the same domain and experiments are shown in Figure 5. Arrows indicate the current direction in the areas with velocity magnitude exceeding 0.1 m s^{-1} . For the R-CTRL pattern (Figure 5a), it is clear that the Kuroshio flows along the southern coast of Japan after passing through the Tokara

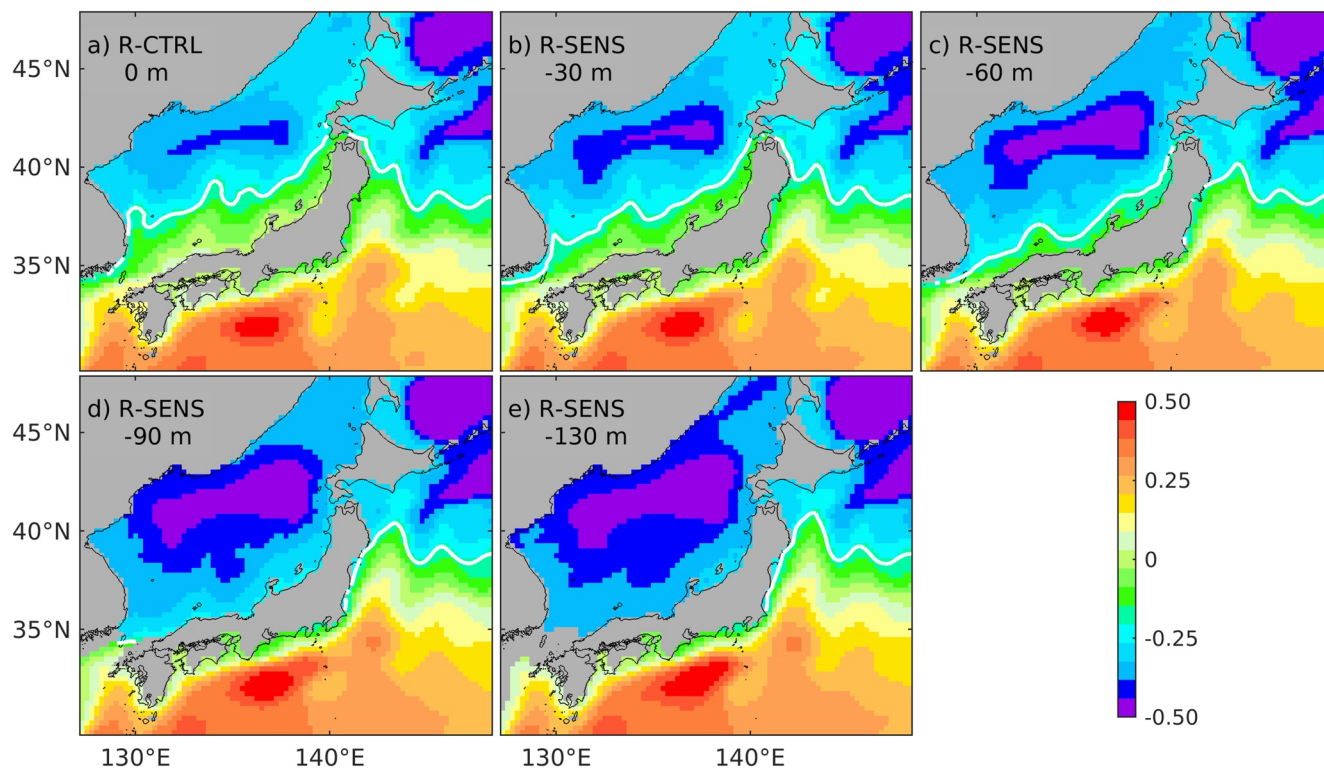


Figure 4. Annual mean elevation (shadings, unit: m) of R-CTRL and R-SENS (–30, –60, –90, and –130 m) around the Japan Sea. White solid lines indicate contour of –0.2 m.

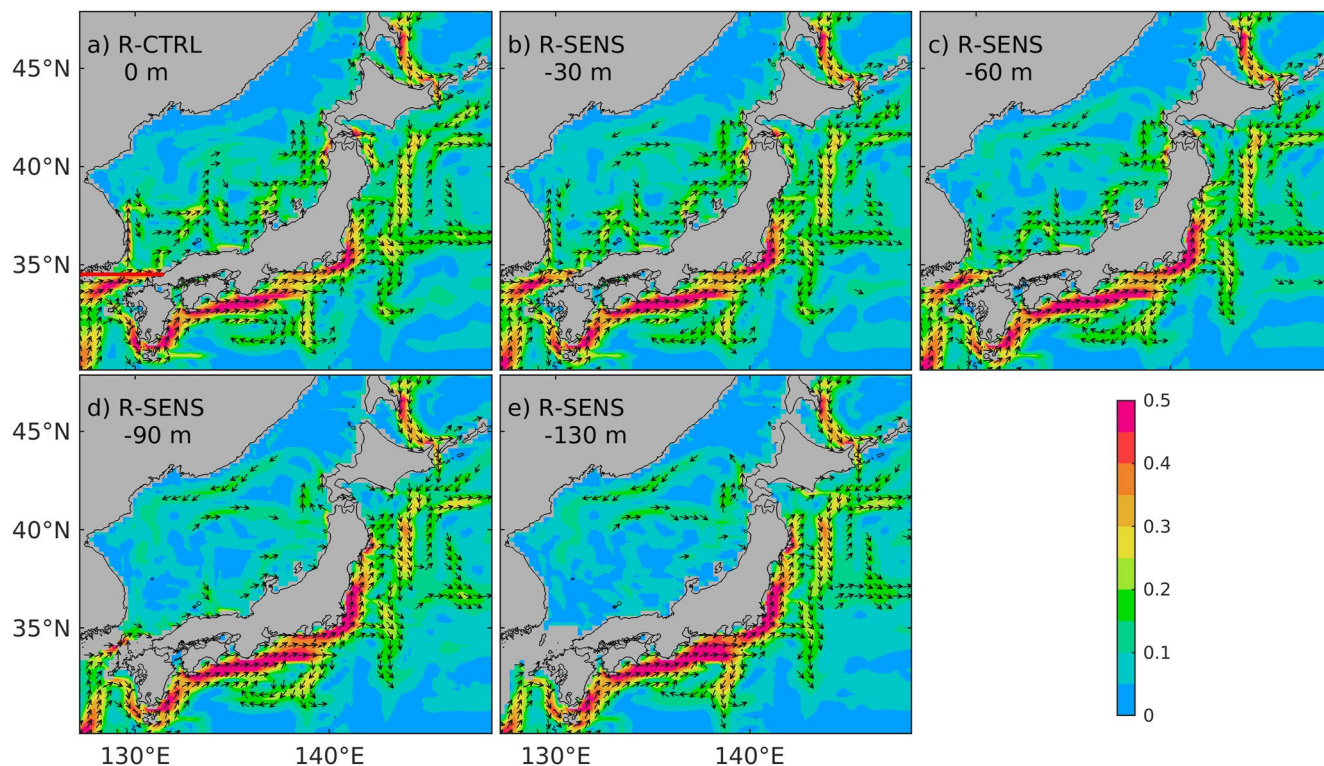


Figure 5. Annual mean sea surface speed (shadings, unit: m s^{-1}) of R-CTRL and R-SENS (–30, –60, –90, and –130 m) around the Japan Sea. Arrows indicate current direction in the area with a speed over 0.1 m s^{-1} . Red line in (a) indicate section for calculating the Tsushima Strait transport.

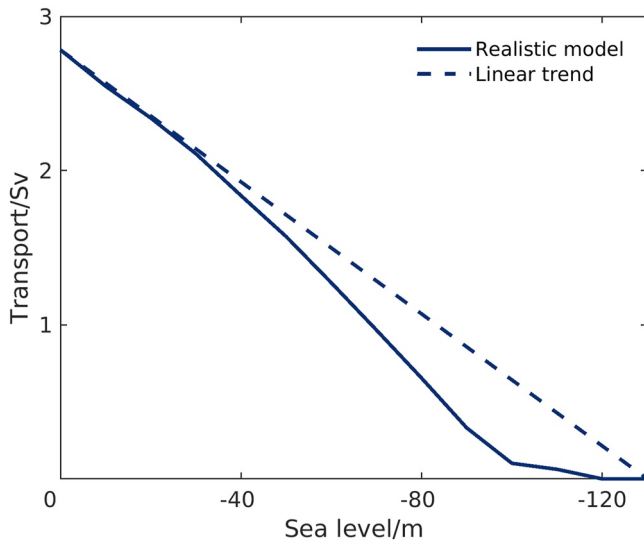


Figure 6. Relationship between Q and sea level. Solid line (non-linear relationship) presents the Q estimated from the R-CTRL (horizontal tick label is 0 m) and R-SENS (horizontal tick label varies from -10 to -130 m) results. Dashed line (linear relationship) links the transport under the sea level at 0 and -130 m as a linear trend reference.

Strait, leaves Honshu Island, and enters the Northwest Pacific as the Kuroshio Extension. With sea level reduction, the Kuroshio is strengthened in velocity and the affected area (extending to the east coast of Honshu Island, Figures 5b–5e). The Tsushima Warm Current, shown in Figures 1b and 5a, is separated into three current branches after entering the Japan Sea. (a) The East Korea Warm Branch flows northward along the eastern coast of the Korean Peninsula and returns to the south, rejoining the Tsushima Warm Current; (b) The Nearshore Branch flows northeastward along the western coast of Kyushu and Honshu Islands and reaches the vicinity of the Tsugaru Strait; and (c) A weak Offshore Branch flows northward between the other two branches, meanders after touching the subpolar front, and organizes itself into the Nearshore Branch. These three branches agree well with previous studies (Chang et al., 2016). In R-SENS results, these current branches likely weaken as the sea level decreased and almost disappear at -130 m sea level due to the cutoff of the Tsushima Strait (Figure 5e). In the northwestern part of the Japan Sea, the Liman Cold Current, flowing along the Siberian coast southward to Vladivostok, is too weak ($<0.1 \text{ m s}^{-1}$) to be identified in the R-CTRL pattern. As the sea level decreases, the Liman Cold Current strengthens, and a cyclonic gyre emerges in the northern part of the Japan Sea (Figures 5b–5e), which is related to the wind stress curl there (D. Kim et al., 2020).

In these sensitivity experiments, the dropping sea level leads a reduction in mean elevation and a variation in the surface circulation pattern in the Japan Sea. The Japan Sea, as a semi-enclosed sea, receives external forcing from

the sea surface and lateral boundaries and its hydrodynamic characteristics therefore are determined by the above two factors. Since the sea surface forcing is unchanged, the only change from the R-CTRL is the eustatic sea level in the sensitivity experiments. The dropping sea level restricts not only the volume transport but also the momentum and heat/salt flux through the Tsushima Strait. As a result, the lateral boundaries contribute less kinetic and buoyancy energy to the formation of the hydrodynamic pattern than the sea surface forcing does. Through these sensitivity experiments, we capture how the eustatic sea level affects the local hydrological conditions.

3.1.2. Non-Linear Regression Relationship Between the Q and Sea Level

The annual mean Q under the present sea level (0 m) in R-CTRL is presented in Figure 6 as a starting point for the reduction of Q with the drop in sea level, and the section used for transport estimation is shown in Figure 5a as a red line. For a quick comparison, the mean transports obtained from long-term in-situ observations are summarized in Table 3. It is known that annual mean Q from R-CTRL (2.78 Sv) is close to the value from the in-situ observations (2.3–2.7 Sv). Therefore, the realistic model can reproduce the mean-state Q under the present sea level, which allows us to use this model to further examine the relationship between Q and sea level.

Figure 6 also shows the response of Q to sea level reduction (solid line) from -10 to -130 m obtained from the R-SENS results. As a reference, we also plot a dashed line linking Q with sea levels at 0 and -130 m, representing a linear downward trend with sea level reduction, that is, the linear regression relationship used by Matsui et al. (1998). The R-SENS results (solid line in Figure 6) demonstrate a steeper downward trend in Q from a sea level of 0 to -100 m, and a gentler downward trend from a sea level of -110 to -130 m as compared to the

linear downward trend (dashed line). Hereinafter, we call the reduction of Q with sea level reduction from the realistic model as the non-linear regression relationship. The potential mechanism for this non-linear relationship will be discussed in Section 4.2.

3.1.3. Evolution of Q

Under this non-linear regression relationship between Q and sea level, we can further convert the sea level evolution proposed by Yokoyama et al. (2018) into Q evolution. The conversion process relies on the tripartite relationship between sea level, Q , and time. The relationship between sea level and Q is the above non-linear regression relationship (solid line in Figure 6). Between

Table 3
Mean-State Transport Through the Tsushima Strait Obtained From In-Situ Observations in Previous Studies

Time periods	Mean transport/Sv	Reference
1999.05–2000.03	~2.3 (northeastern section) ~2.7 (southwestern section)	Teague et al. (2002)
1997.02–2002.08	~2.64	Takikawa et al. (2005)
1997.02–2007.02	~2.65	Fukudome et al. (2010)

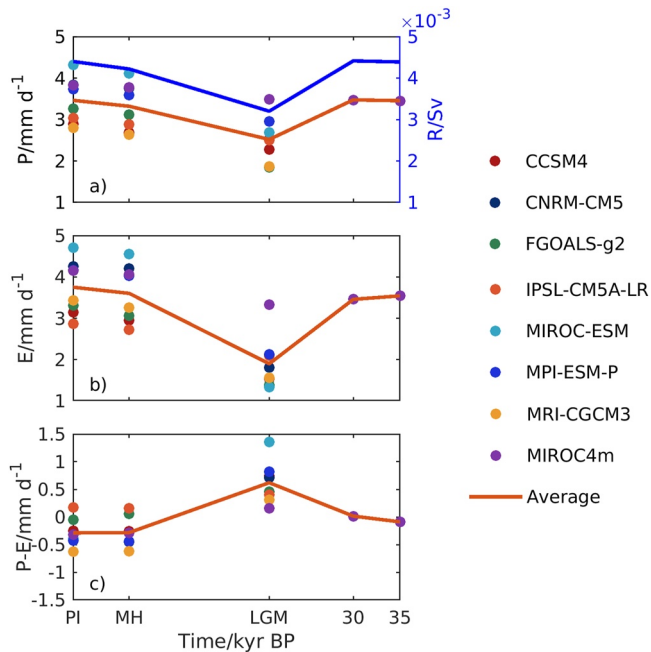


Figure 7. The precipitation (P) and river discharge (R), evaporation (E), and precipitation minus evaporation ($P-E$) evolutions. (a), (b), and (c) exhibit P and R , E , and $P-E$ over the Japan Sea, respectively. A positive value of $P-E$ indicates freshwater flux into the Japan Sea through the air-sea interface. In each panel, the filled dots with the same color represent the value of a variable (left vertical axis) at PI, MH, LGM, 30, and 35 kyr BP. Different colors indicate different model results from PMIP3 and MIROC4m, and the corresponding relationship between color and model name can be found in the right legend. The solid orange lines represent the average value over these multi-model results.

sea level and time is referred to sea level evolution by Yokoyama et al. (2018; Figure 3a). By coupling these two relationships, the relationship between Q and time, that is, the Q evolution, is obtained (solid line in Figure 3b). The main features of the Q evolution are as follows: (a) 35–32 kyr BP, transport decreases slightly from about 1.15 to 1.0 Sv; (b) 31–29 kyr BP, the rate of reduction becomes greater from about 1.0 to 0.1 Sv; (c) 28–16 kyr BP, the transport is smaller than 0.1 Sv with a fairly small fluctuation. The Tsushima Strait is almost closed around the LGM period when transport is close to zero; (d) 15–3 kyr BP, the Tsushima Strait reopens with sea level rising and the transport increases rapidly to about 2.76 Sv; and (e) 2 kyr BP–Present, the transport remains at about 2.78 Sv. The width of the curve in Figure 3b represents analytical uncertainties from sea level.

With the same process, the Q evolution can also be converted from sea level evolutions in Saito et al. (1998) and Arz et al. (2007) (Figures 3d and 3f, respectively). It is found that from 35 to 25 kyr BP, the features from these three Q evolutions are quite different: a general downward trend for that based on Yokoyama et al. (2018) and Arz et al. (2007), but a roughly upward and then downward trend for that based on Saito et al. (1998). Subsequently, these three Q evolutions exhibit similar features, remaining at almost zero throughout 25–15 kyr BP and increasing after 15 kyr BP.

We apply the Q evolution converted from Yokoyama et al. (2018) sea level data to reconstruct S_{JP} over the past 35 kyr, and those from Saito et al. (1998) and Arz et al. (2007) to discuss the influence of Q on the minimum S_{JP} .

3.2. $P-E$ Evolution

The evolutions of precipitation and evaporation obtained from multi-model simulation results are shown in Figures 7a and 7b, respectively. At 35 and 30 kyr BP, only the results from the MIROC4m model are available, and both the precipitation (~ 3.4 mm d^{-1}) and evaporation (~ 3.4 mm d^{-1}) remained stable at these two periods. From the LGM to the PI, the PMIP3 model results are also available, and all the models suggest an increasing trend in precipita-

tion and evaporation. It should be noted that the specific values of precipitation and evaporation vary from model to model. The mean precipitation and evaporation, calculated from the available model results for each period, are shown using solid orange lines in Figures 7a and 7b, respectively. Both the mean precipitation and evaporation are minimal (2.52, 1.90 mm d^{-1}) during the LGM with a roughly downward (upward) trend before (after) the LGM, which is related to the reduction of air temperature and weakening of solar radiation.

Figure 7c shows the $P-E$ evolutions from the multi-model simulation results with their averaged values (a positive value indicates freshwater entering the Japan Sea through the air-sea interface). An upward trend in $P-E$ is found from 35 kyr BP to the LGM. As for the period from the LGM to the PI, the mean $P-E$ exhibits a downward trend until it stabilizes after the MH. The mean $P-E$ has its maximum value (0.62 mm d^{-1}) at the LGM, which is smaller than that (0.82 mm d^{-1}) in Matsui et al. (1998) and Ikeda et al. (1999).

To minimize model uncertainties, the $P-E$ evolution averaged over the multi-model simulation results is used to force the box model. The $P-E$ evolution from each model is employed individually to explore the influence of $P-E$ on the minimum S_{JP} .

As we assumed that $R(t)$ is linearly proportional to $P(t)$, the variation of river discharge is similar to that of precipitation as shown in Figure 7a. Here, α is 0.0013 Sv $mm^{-1} d$ calculated as the ratio of presented-day river discharge (0.0044 Sv, Yanagi, 2002) and precipitation (3.46 mm d^{-1} , averaged over the PMIP3 and MIROC simulations for PI).

3.3. S_{JP} Evolution

The Q evolution converted from sea level in Yokoyama et al. (2018) under the non-linear regression relationship, and $P-E$ evolution averaged from multi-model simulation results, are employed to drive the box model. The

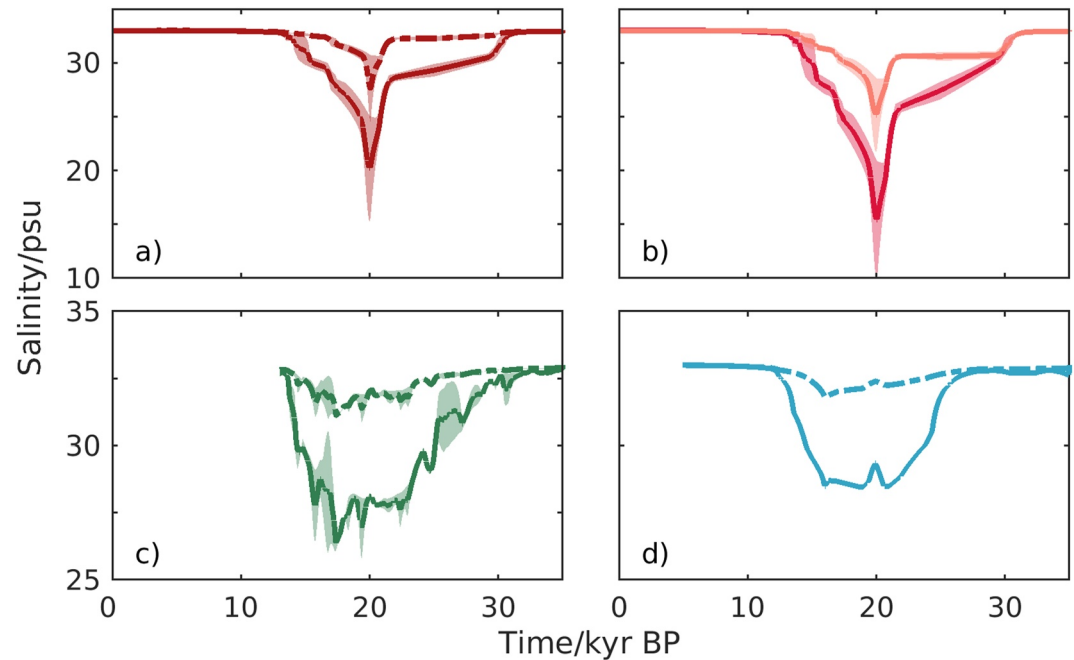


Figure 8. S_{jp} evolution reconstructed from the box model. The solid (dashed) line in (a) is the result forced by Q evolution under the non-linear (linear) relationship, and averaged $P-E$ evolution. The sea level evolution used here is adapted from Yokoyama et al. (2018). The solid red (pink) line in (b) is the result forced by the $P-E$ evolution obtained from MIROC-ESM (MIROC4m) model, and Q evolution converted from sea level in Yokoyama et al. (2018) under the non-linear relationship. The solid/dashed lines in (c) and (d) are the same as that in (a), but the sea level evolutions used here are adapted from Arz et al. (2007) and Saito et al. (1998), respectively. Width of the curve represents typical uncertainties from sea level.

reconstructed S_{jp} evolution over the past 35 kyr using Equation 1 is shown in Figure 8a as a solid line. During the period of 35–31 kyr BP, the reconstructed S_{jp} maintains its initial value (32.8) with slight fluctuations (<0.2) because of stable inflow transport and weak freshwater flux. From 31 kyr BP until the timing of minimum S_{jp} (20 kyr BP), there are three distinct stages of S_{jp} decline: falling abruptly from 32.8 to 30 during 31–29 kyr BP, decreasing gently from 30 to 28.6 during 29–22 kyr BP, and dropping sharply from 28.6 to the minimum S_{jp} (20.2) during 22–20 kyr BP. As shown in Section 4.3, it is the combined effect of weaker inflow transport and heavier freshwater flux that leads to minimum S_{jp} (20.2) around 20 kyr BP. Meanwhile, a robust halocline is expected at 20 kyr BP, and this separates the seawater of the Japan Sea into two main layers with a less saline upper layer and a more saline lower layer (Isobe, 2020). From then on, S_{jp} begins to rise gradually with the reopening of the Tsushima and Tsugaru Straits and a reduction of freshwater flux. S_{jp} recovers its initial value at 13 kyr BP and this persists until the present. Overall, the reconstructed S_{jp} reaches its minimum value of 20.2 at 20 kyr BP, which is close to that estimated by Matsui et al. (1998) (20 at 20–15 kyr BP).

Additionally, linear regression analysis is conducted to explore the relationship between $\delta^{18}O$ and the reconstructed S_{jp} (Figure 9a), and the coefficient of determination (R^2) is used to evaluate the correlation between them. The $\delta^{18}O$ evolution used here is adapted from Sagawa et al. (2018), as shown in Figures 1c and is estimated from *Globigerina bulloide* of the KR07-12 PC3 core located in the southern Japan Sea. It is found that the slope and intercept for the linear relationship between reconstructed S_{jp} and $\delta^{18}O$ are 0.22 and -4.50 , respectively. A high value of R^2 (0.81, $p \ll 0.01$) indicates that the reconstructed S_{jp} is significant correlated with $\delta^{18}O$ and describes the low S_{jp} event in the Japan Sea reasonably well.

4. Discussion

In this section, the necessity of the non-linear regression relationship for S_{jp} reconstruction is clarified and the mechanism behind this non-linear relationship is explored. Next, we reveal the cause of the minimum S_{jp} and the influence of Q and $P-E$ evolutions on it. At last, the implications of changing in Q and S_{jp} on the Japan Sea are discussed.

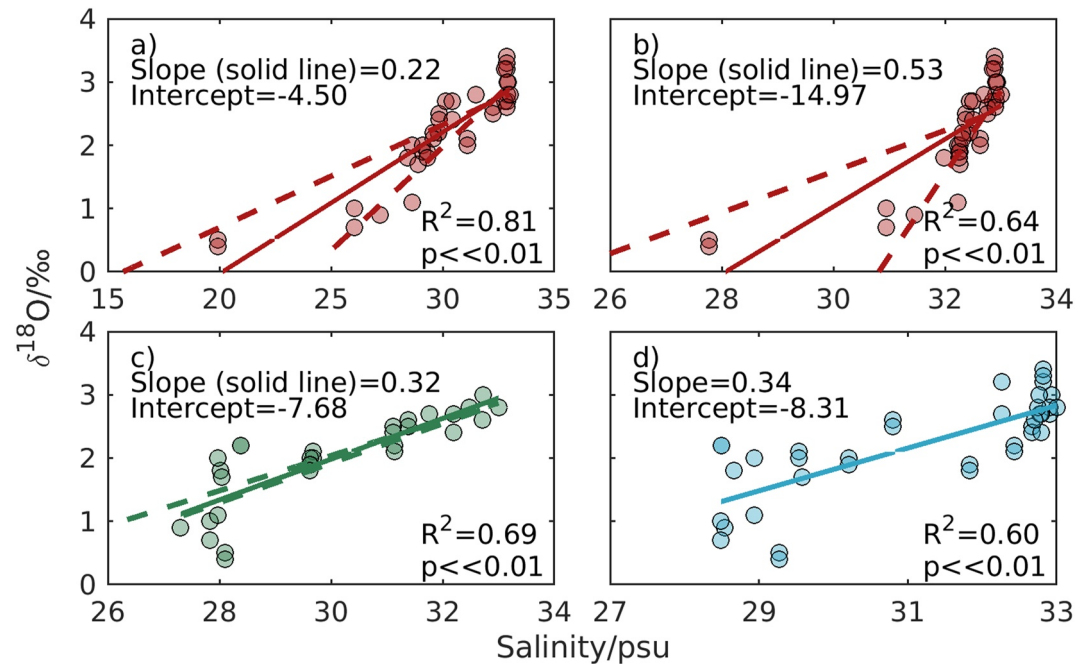


Figure 9. Linear regression of $\delta^{18}\text{O}$ and reconstructed S_{JP} evolution. The dots in (a) exhibit the relationship between the $\delta^{18}\text{O}$ and reconstructed S_{JP} evolution. Here, S_{JP} evolution is reconstructed with the Q evolution converted from Yokoyama et al. (2018) sea level under the non-linear relationship, and averaged $P-E$ evolution. The solid line is a linear regression of these dots, and dashed lines represent typical uncertainties from sea level. (b) exhibits the relationship between the $\delta^{18}\text{O}$ and reconstructed S_{JP} evolution, but the Q evolution is converted under the linear regression relationship. (c) and (d) exhibit the relationship between the $\delta^{18}\text{O}$ and reconstructed S_{JP} evolution, but the Q evolution is converted from Arz et al. (2007) and Saito et al. (1998) sea level, respectively.

4.1. Necessity of the Non-Linear Regression Relationship

By coupling the Q evolution converted under a non-linear relationship and $P-E$ evolution averaged over the multi-model simulation results, the S_{JP} evolution has been reconstructed using the box model and its R^2 for $\delta^{18}\text{O}$ is estimated to be 0.81 ($p < < 0.01$). Here, we demonstrate that a non-linear relationship promises such a precise result.

To clarify the necessity of this non-linear relationship, we reconstruct the S_{JP} evolution again with the same setting, but convert the Q evolution under the linear relationship (dashed line in Figure 6) assumed by Matsui et al. (1998). Similarly, the sea level evolution used here is also adapted from Yokoyama et al. (2018). The Q evolution converted under the linear relationship is shown in Figure 3b using the dashed line, and its values are generally much larger than those under the non-linear relationship, except for the period from 10 kyr BP to the present.

Figure 8a presents the S_{JP} evolution forced by this “linear” Q evolution in the dashed line. It exhibits much higher values and less variation than that forced by the “non-linear” Q evolution (solid line in Figure 8a). This new S_{JP} evolution reaches its minimum value (27.7), which is larger than the previous value (20.2), but occurs at the same time, 20 kyr BP. Further linear regression analysis suggests that the value of R^2 (0.64, $p < < 0.01$; Figure 9b) for this new S_{JP} evolution is smaller than the previous one (0.81, $p < < 0.01$; Figure 9a), which indicates that the former, forced by the “linear” Q evolution, cannot describe the variability in $\delta^{18}\text{O}$ as sufficiently as the latter. Additionally, the sea level elevations from Arz et al. (2007) and Saito et al. (1998) are also employed to carry out the same experiments, and the results (not shown here) also lead to the same conclusions. In this sense, the non-linear regression relationship is more suitable for S_{JP} reconstruction than linear. It is necessary to refine Q evolution using this non-linear regression relationship when dealing with the paleo Japan Sea.

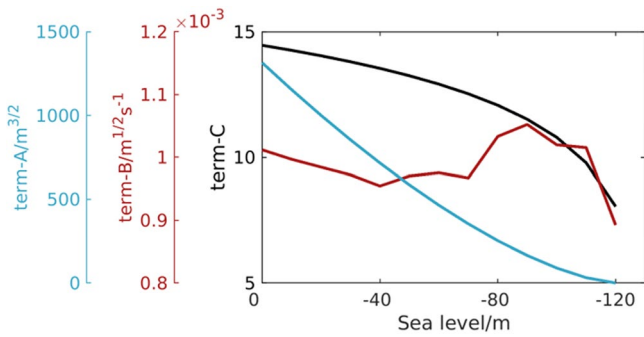


Figure 10. Variations of term-A, B, and C split from Equation 3 with sea level dropping.

4.2. Cause for the Non-Linear Regression Relationship

We have employed realistic bathymetry and meteorological forcing to investigate Q and its non-linear mapping relationship with sea level. An interesting question is why there is a non-linear response for Q to sea level change rather than a linear one as assumed in Matsui et al. (1998)? Generally, if the Tsushima Strait is regarded as a channel with uniform depth h , length L , and width B connecting two large basins, then its mean-state transport can be derived from the along-strait (x -direction) momentum balance, as follows:

$$Q = Bhu_a = B \overbrace{h^{3/2}}^{\text{term-A}} \left(-g \frac{\partial \eta}{\partial x} \right)^{1/2} \overbrace{C_d^{-1/2}}^{\text{term-C}} \quad (3)$$

where u_a is the depth-averaged velocity component in the along-strait direction, g is gravitational acceleration, η is surface elevation, and C_d is the bottom friction coefficient. The derivation of Equation 3 is given in the Text S3 in Supporting Information S1.

Equation 3 depicts a non-linear relationship between Q and sea level (strait depth h) assuming that other terms vary little with water depth. With output data from the realistic model, we can estimate each term in Equation 3 and diagnose these effects on the non-linearity. However, multiple spatial-scale variations are contained in both the topographical and regional meteorological forcings. The hotchpotch of multiscale variations may sometimes blur the dominant dynamical processes (Yang & Pratt, 2013) and, as a result, complicate the diagnosis of Equation 3. Therefore, we build a simple but more general finite-depth idealized numerical model to bring insight into why Q responds non-linearly to the sea level change. The configurations of this finite-depth idealized model can be found in the Text S4 in Supporting Information S1. Text S5 suggests that a similar non-linear relationship could be mirrored by the results from this idealized model and is formulated by Equation 3, which increases our confidence in diagnosing Equation 3 with the output from this idealized model.

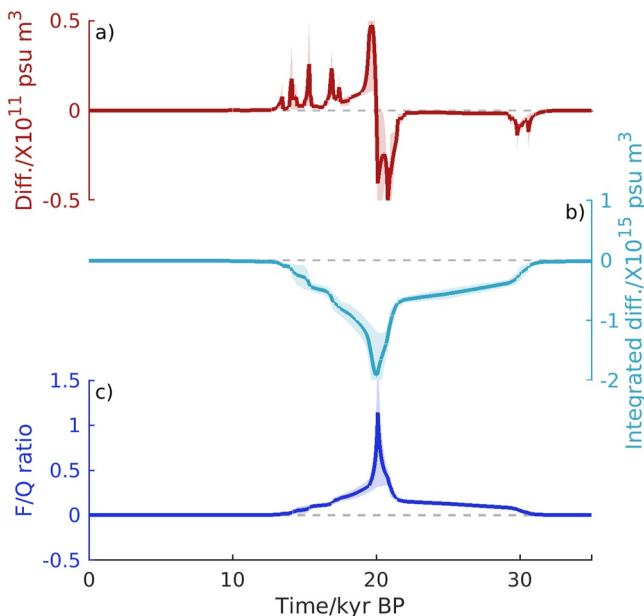


Figure 11. (a) The differences between salt input and output over the past 35 kyr. The dashed line denotes the zero line for reference. Width of the curve represents typical uncertainties from sea level. (b) and (c) are the same as (a) but for time-integrated salt differences and ratio of freshwater flux and Tsushima Strait transport (F/Q), respectively.

The changes in each term in Equation 3 with sea level reduction are shown in Figure 10. Term-A, which represents the strait depth to the power of $3/2$, exhibits a non-linear downward trend, similar to the transport response to sea level reduction. However, term-B, representing the elevation difference across the strait, shows an irregular behavior with slight fluctuations. Term-C, representing C_d to the power of $-1/2$, shows a non-linear and downward trend because C_d is inversely proportional to the sea level. However, the variation range of term-C is much smaller than that of term-A. Therefore, it is the variation in term-A that contributes to the majority of the non-linear downward variation, and it can be concluded that term-A, $h^{3/2}$, plays a dominant role in determining the non-linear regression relationship.

4.3. Cause of the Minimum S_{JP} in 20 kyr BP

In the box model for salinity, the differences between salt input and output regulate the salinity inside the box and the time-cumulative differences determine the salinity evolution. For the Japan Sea, the transport through the Tsushima Strait provides salt into the Japan Sea. Meanwhile, the transport through the Tsugaru and Soya Straits together with the freshwater flux serves as the main salt output. To specifically explain the appearance of the minimum S_{JP} (20.2) at 20 kyr BP, we plot the difference between salt input and output, its time-integrated value, and the ratio of freshwater flux and transport through the Tsushima Strait (F/Q) over the past 35 kyr (Figure 11).

From 35 to 20 kyr BP, the difference between salt input and output is less than or equal to zero (Figure 11a), which suggests the salt input from the Tsushima Strait is in short supply to the salt output through the Tsugaru and Soya Straits. Over this period, the transport through the Tsushima Strait decreased

to almost zero and in contrast, the freshwater flux increased to a peak value, which together led to a decreasing S_{JP} . The descending time-integrated difference also indicates a continued salt loss until 20 kyr BP (Figure 11b).

Around 20 kyr BP, the transport through the Tsushima Strait decreased to almost the same amount of freshwater flux but then recovered back quickly (Figure 11c), leading the difference between the salt input and output to change suddenly from a negative value to a positive value (Figure 11a).

After the 20 kyr BP, the difference was greater than or equal to zero (Figure 11a), which runs a salt budget surplus with the increasing of transport through the Tsushima Strait and decreasing of freshwater flux. The S_{JP} thereby increases with time. The time-integrated difference changed from decreasing to increasing, which suggests a salt gain after 20 kyr BP (Figure 11b). The minimum S_{JP} therefore occurs at the break-even point when the F/Q reached a maximum value, that is, 20 kyr BP (Figure 11c). It is concluded that the combination of the volume transport through the Tsushima Strait and the freshwater input determines the exact value and timing of minimum salinity.

4.4. Impact of Q Evolution on the Minimum S_{JP}

Under the non-linear regression relationship, the Q evolution has been determined by the sea level evolution in Yokoyama et al. (2018) and further applied to reconstruct the S_{JP} evolution. To further analyze the effect of the Q evolution on the minimum S_{JP} , we also convert the sea level evolutions in Arz et al. (2007) and Saito et al. (1998) into Q evolution and rerun the box model with the averaged $P-E$ evolution. The corresponding results of the S_{JP} evolution are shown in Figures 8c and 8d, respectively. Combining the results forced by Q evolution under Yokoyama et al. (2018) sea level (solid line in Figure 8a), it is found that these three types of S_{JP} evolutions are all roughly axisymmetric over the past 35 kyr, that is, a downward (upward) trend before (after) ~ 20 kyr BP with a minimum value around this period. Notably, the exact value and timing of minimum S_{JP} for these three evolutions are different: a minimum value of ~ 20.2 , ~ 26.4 , and 28.4 at 20, 17, and 19 kyr BP for Q evolution converted from Yokoyama et al. (2018), Arz et al. (2007), and Saito et al. (1998) sea level, respectively, which indicates that Q evolution plays a crucial role in determining both the value and timing of the minimum S_{JP} . These timings correspond to the moments when the F/Q reaches a maximum value, suggesting again the combined effect of freshwater flux and transport through the Tsushima Strait on the appearance of minimum S_{JP} .

Linear regression analysis for $\delta^{18}\text{O}$ and S_{JP} evolution, corresponding to Q evolutions converted from Arz et al. (2007) and Saito et al. (1998) sea level, are shown in Figures 9c and 9d, respectively. The value of R^2 for these two S_{JP} evolutions (0.69, 0.60; $p \ll 0.01$) are both smaller than that shown in Figure 9a (0.81, $p \ll 0.01$), which means that the Q evolution converted from Yokoyama et al. (2018) sea level is the most suitable for S_{JP} reconstruction. This also reminds us that it is still valuable and desirable to explore an accurate sea level evolution.

4.5. Impact of $P-E$ Evolution on the Minimum S_{JP}

We would also like to discuss the influence of $P-E$ evolution on the value and timing of the minimum S_{JP} . Here, the Q evolution is converted from the Yokoyama et al. (2018) sea level under the non-linear regression relationship, and the $P-E$ evolution is obtained from each PMIP3 and MIROC4m simulation result, one by one. Therefore, eight types of $P-E$ evolutions are used to drive the box model with the same Q evolution.

It is found that each type of reconstructed S_{JP} suggests a similar evolution feature to that forced by the averaged $P-E$ evolution, that is, a minimum S_{JP} around ~ 20 kyr BP with a considerable descending and rising process before and after, respectively. Thus, only the S_{JP} evolutions corresponding to the MIROC-ESM and MIROC4m simulations are selected and shown in Figure 8b as red and pink lines, respectively. Results corresponding to the other six models lie somewhere between these two and are omitted here. Notably, the $P-E$ evolution data for 35–30 kyr BP from the PMIP3 models are not available, and those from the MIROC4m model replace them. As a result, the reconstructed S_{JP} evolutions from 35 to 30 kyr BP are the same as that in Figure 8a. All the reconstructed S_{JP} under $P-E$ evolutions from CCSM4, CNRM-CM5, FGOALS-g2, IPSL-CM5A-LR, MIROC-ESM, MPI-ESM-P, MRI-CGCM3, and MIROC4m models produce their minimum values (19.21, 19.53, 21.52, 22.08, 15.45, 18.71, 23.49, and 25.17, respectively) around 20 kyr BP, which means that the $P-E$ evolution can modify only the value of minimum S_{JP} but not the timing. In other words, the Q evolution, adjusted by the eustatic sea level, determines the amount of saline water entering the Japan Sea and mostly determines the value and timing of the minimum S_{JP} . Meanwhile, the $P-E$ evolution provides a continuous freshwater supply to modify the value of minimum S_{JP} .

4.6. Implications of the Changes in Q and S_{JP} on the Japan Sea

In the present configuration, the inflow through the shallow Tsushima Strait brings warm and saline water into the Japan Sea, which significantly affects the hydrography of the upper layer water (Dong et al., 2021). The deep layer is occupied by a water mass called the Japan Sea Proper Water, which is formed by deep convection due to surface cooling under the winter East Asian Monsoon in the northern Japan Sea (Senjyu, 2022). The semi-isolation and self-contained thermohaline circulation system including deep water formation make the Japan Sea unique among the various marginal seas in the western North Pacific (Kida et al., 2016; Wu et al., 2020).

Over the past 35 kyr BP, the eustatic sea level would have regulated the inflow through the Tsushima Strait and thereby the surface salinity of the Japan Sea (Dong et al., 2020; Tada et al., 2018). During the glacial period, especially during the LGM, the inflow through the Tsushima Strait, restricted by the dropping sea level, was in short supply of the salt input to the Japan Sea. Moreover, the occurrence of dropstones and ice-rafted debris indicates active sea ice formation in the northern Japan Sea during this interval (Ikehara, 2003). Together with the continuous freshwater water supply, a lower-salinity sea surface is formed. Since the deep water is formed by the surface cooling and deep convection, the lower salinity surface water could enhance the density stratification of the water column and severely limit the occurrence of deep convection as well as the formation of deep water. The benthic foraminiferal barren zone accompanied by high concentrations of sedimentary molybdenum suggests the existence of a poorly ventilated deep-water in the Japan Sea (Domitsu & Oda, 2006; Dong et al., 2021). The dissolved oxygen would be consumed up through oxidation of organic material, and the anoxic and sulfidic bottom conditions have been developed in the deep water (Ishiwatari et al., 2001; Keigwin & Gorbarenko, 1992), which has been indicated by the presence of well-laminated sediment (Watanabe et al., 2007) and peak values of total sulfur/organic carbon (TS/TOC) (Zou et al., 2012). The sea level rise since the LGM leads to the reopening of the Tsushima and Tsugaru Straits. The stratification in the Japan Sea then weakened and the ventilation became possible again. The reemergence of microfossils in the marine sediment cores indicates that the benthic fauna have recovered with the oxygen supply from the upper water to the deep water (Itaki et al., 2004). In addition, the present-day Japan Sea is a net sink for atmospheric CO_2 (M. Kim et al., 2022) and the hypoxic deep/bottom waters in the glacial period have been considered as a potential carbon source to the atmosphere (Dong et al., 2021; D. Li et al., 2019). With the re-ventilation since the LGM, the changing role of the Japan Sea in the carbon cycle deserves further study.

5. Summary

Using a simple box model, the low sea surface salinity event of the Japan Sea during the LGM is investigated through two indicators: the value and timing of the minimum S_{JP} . As a cornerstone, the relationship between Q and sea level is quantified. A non-linear regression relationship, rather than the linear one assumed in Matsui et al. (1998), is confirmed through a dynamically-constrained realistic numerical model and experiments with different sea levels. Assisted by this non-linear regression relationship, the sea level evolution reported in previous studies can be converted into Q evolution to force the box model. We also refine the $P-E$ evolution with simulation results from seven PMIP3 models and from MIROC4m.

Forced by the Q evolution converted from Yokoyama et al. (2018) sea level under the above non-linear relationship and $P-E$ evolution averaged over these multi-model simulation results, the S_{JP} evolution is reconstructed with the box model, and a minimum value (20.2) is reached 20 kyr BP (solid line in Figure 8a). A high value of R^2 (0.81, $p \ll 0.01$) for $\delta^{18}\text{O}$ evolution suggests a high degree of reliability for this S_{JP} evolution.

A comparison experiment is conducted by converting the Q evolution under the linear regression relationship, and a smaller R^2 (0.64, $p \ll 0.01$) demonstrates that the non-linear relationship is essential for S_{JP} reconstruction. Analysis through Equation 3 and an idealized numerical model reveal that the dependence of Q on $h^{3/2}$ is the cause of this non-linear relationship.

The combined effect of Q and $P-E$ determines the occurrence of minimum S_{JP} . Furthermore, we discuss the impact of Q and $P-E$ evolutions on the minimum S_{JP} . Under the averaged $P-E$ evolution, the reconstructed S_{JP} evolutions, forced by Q evolution converted from sea level in Yokoyama et al. (2018), Arz et al. (2007), and Saito et al. (1998), reached minimum values of ~ 20.2 , ~ 26.4 , and 28.4 at 20, 17, and 19 kyr BP, respectively. Meanwhile, under the Q evolution converted from Yokoyama et al. (2018) sea level, all of the reconstructed S_{JP} evolutions forced by $P-E$ evolution from different models exhibited their minimum S_{JP} at 20 kyr BP, but the

minimum values are quite different. The Q evolution likely dominates both the value and timing of the minimum S_{jp} , whereas $P-E$ evolution modifies its value.

In summary, the refinement of Q and $P-E$ evolutions by using the box model deepens our knowledge of the low sea surface salinity event of the Japan Sea. With innovations in theoretical methodology, developments of paleoclimate numerical models, and enrichments of proxy data, a more comprehensive and profound understanding of the paleo Japan Sea is expected in the future.

Data Availability Statement

Configurations of the box model, the realistic numerical model, and the finite-depth idealized numerical model are available in Miyazawa et al. (2009), Jordi and Wang (2012) and Yang et al. (2022). Evolution of oxygen isotopic ratio in planktonic foraminifera is adapted from Sagawa et al. (2018). Evolutions of sea level are adapted from Yokoyama et al. (2018), Arz et al. (2007), and Saito et al. (1998). The basic information about the PMIP3 and MIROC4m models is listed in Table 2. Simulation results from the PMIP3 models can access by searching in <https://esgf-node.ipsl.upmc.fr/search/esgf-ips/>. The MIROC4m data used in this study are available at Zheng et al. (2022).

Acknowledgments

This work was supported by JSPS KAKENHI Grants 17H02959, 17H06104, and 17H06323. Junyong Zheng thanks the financial support from China Scholarship Council (CSC, No. 202006330055) for supporting his stay in Japan.

References

- Arz, H. W., Lamy, F., Ganopolski, A., Nowaczyk, N., & Patzold, J. (2007). Dominant Northern Hemisphere climate control over millennial-scale glacial sea-level variability. *Quaternary Science Reviews*, 26(3–4), 312–321. <https://doi.org/10.1016/j.quascirev.2006.07.016>
- Braconnot, P., Harrison, S. P., Kageyama, M., Bartlein, P. J., Masson-Delmotte, V., Abe-Ouchi, A., et al. (2012). Evaluation of climate models using palaeoclimatic data. *Nature Climate Change*, 2(6), 417–424. <https://doi.org/10.1038/nclimate1456>
- Chan, W.-L., Abe-Ouchi, A., & Ohgaito, R. (2011). Simulating the mid-pliocene climate with the MIROC general circulation model: Experimental design and initial results. *Geoscientific Model Development*, 4, 1035–1049. <https://doi.org/10.5194/gmd-4-1035-2011>
- Chang, K.-I., Zhang, C.-I., Park, C., Kang, D. J., Ju, S. J., Lee, S. H., et al. (Eds.) (2016). *Oceanography of the East Sea (Japan Sea)*. Springer International Publishing.
- Clark, P. U., Dyke, A. S., Shakun, J. D., Carlson, A. E., Clark, J., Wohlfarth, B., et al. (2009). The Last Glacial Maximum. *Science*, 325(5941), 710–714. <https://doi.org/10.1126/science.1172873>
- Domitsu, H., & Oda, M. (2006). Linkages between surface and deep circulations in the southern Japan Sea during the last 27,000 years: Evidence from planktic foraminiferal assemblages and stable isotope records. *Marine Micropaleontology*, 61(4), 155–170. <https://doi.org/10.1016/j.marmicro.2006.06.006>
- Dong, Z., Shi, X., Zou, J., Chen, M., Zhang, Q., Kandasamy, S., et al. (2020). Drastic hydrographic changes inferred from radiolarian assemblages in the central Japan Sea since the Last Glacial Maximum. *Marine Geology*, 429, 106295. <https://doi.org/10.1016/j.margeo.2020.106295>
- Dong, Z., Shi, X., Zou, J., Dou, R., Wu, Y., Liu, Y., et al. (2021). Paleoceanographic insights on meridional ventilation variations in the Japan Sea since the Last Glacial Maximum: A radiolarian assemblage perspective. *Global and Planetary Change*, 200, 103456. <https://doi.org/10.1016/j.gloplacha.2021.103456>
- Dufresne, J.-L., Foujols, M.-A., Denvil, S., Caubel, A., Marti, O., Aumont, O., et al. (2013). Climate change projections using the IPSL-CM5 Earth System Model: From CMIP3 to CMIP5. *Climate Dynamics*, 40(9–10), 2123–2165. <https://doi.org/10.1007/s00382-012-1636-1>
- Fairbanks, R. G. (1989). A 17,000-year glacio-eustatic sea level record: Influence of glacial melting rates on the Younger Dryas event and deep-ocean circulation. *Nature*, 342(6250), 637–642. <https://doi.org/10.1038/342637a0>
- Fujie, K., Tada, R., & Yamamoto, M. (2009). Paleotemperature response to monsoon activity in the Japan Sea during the last 160kyr. *Paleoceanography, Palaeoclimatology, Palaeoecology*, 280(3–4), 350–360. <https://doi.org/10.1016/j.palaeo.2009.06.022>
- Fukudome, K.-I., Yoon, J.-H., Ostrovskii, A., Takikawa, T., & Han, I. S. (2010). Seasonal volume transport variation in the Tsushima Warm Current through the Tsushima Straits from 10 years of ADCP observations. *Journal of Oceanography*, 66(4), 539–551. <https://doi.org/10.1007/s10872-010-0045-5>
- Gamo, T., Nakayama, N., Takahata, N., Sano, Y., Zhang, J., Yamazaki, E., et al. (2014). The Sea of Japan and its unique chemistry revealed by time-series observations over the last 30 years. *Monographs on Environment, Earth and Planets*, 2, 1–22. <https://doi.org/10.5047/meep.2014.00201.0001>
- Gent, P. R., Danabasoglu, G., Donner, L. J., Holland, M. M., Hunke, E. C., Jayne, S. R., et al. (2011). The community climate system model version 4. *Journal of Climate*, 24(19), 4973–4991. <https://doi.org/10.1175/2011JCLI4083.1>
- Giorgetta, M. A., Jungclaus, J., Reick, C. H., Legutke, S., Bader, J., Bottinger, M., et al. (2013). Climate and carbon cycle changes from 1850 to 2100 in MPI-ESM simulations for the Coupled Model Intercomparison Project phase 5. *Journal of Advances in Modeling Earth Systems*, 5(3), 572–597. <https://doi.org/10.1002/jame.20038>
- Gorbarenko, S., Shi, X., Bosin, A., Liu, Y., Artemova, A., Zou, J., et al. (2021). Timing and mechanisms of the formation of the dark layers in the Sea of Japan during the last 40 kyr. *Frontiers of Earth Science*, 9, 410. <https://doi.org/10.3389/feart.2021.647495>
- Gorbarenko, S. A., & Southon, J. R. (2000). Detailed Japan Sea paleoceanography during the last 25 kyr: Constraints from AMS dating and $\delta^{18}\text{O}$ of planktonic foraminifera. *Paleoceanography, Palaeoclimatology, Palaeoecology*, 156(3–4), 177–193. [https://doi.org/10.1016/S0031-0182\(99\)00137-6](https://doi.org/10.1016/S0031-0182(99)00137-6)
- Gowan, E. J., Zhang, X., Khosravi, S., Rovere, A., Stocchi, P., Hughes, A. L. C., et al. (2021). A new global ice sheet reconstruction for the past 80,000 years. *Nature Communications*, 12(1), 1199. <https://doi.org/10.1038/s41467-021-21469-w>
- Harrison, S. P., Bartlein, P. J., Izumi, K., Li, G., Annan, J., Hargreaves, J., et al. (2015). Evaluation of CMIP5 palaeo-simulations to improve climate projections. *Nature Climate Change*, 5(8), 735–743. <https://doi.org/10.1038/nclimate2649>
- Hyun, S., Kim, J.-M., Yim, U. H., Shim, W. J., Yoon, S. H., & Woo, K. S. (2013). Variations in sea surface temperatures based on alkenones in Korea Plateau sediments of the East Sea (Sea of Japan) over the last 300,000 years. *Journal of Asian Earth Sciences*, 66, 140–149. <https://doi.org/10.1016/j.jseas.2012.12.036>

- Ikeda, M., Suzuki, F., & Oba, T. (1999). A box model of glacial-interglacial variability in the Japan Sea. *Journal of Oceanography*, 55(4), 483–492. <https://doi.org/10.1023/A:1007831122343>
- Ikehara, K. (2003). Late quaternary seasonal sea-ice history of the northeastern Japan Sea. *Journal of Oceanography*, 59(5), 585–593. <https://doi.org/10.1023/B:JOCE.0000009588.49944.3d>
- Ishiwatari, R., Houtatsu, M., & Okada, H. (2001). Alkenone-sea surface temperatures in the Japan Sea over the past 36 kyr: Warm temperatures at the Last Glacial Maximum. *Organic Geochemistry*, 32(1), 57–67. [https://doi.org/10.1016/S0146-6380\(00\)00151-0](https://doi.org/10.1016/S0146-6380(00)00151-0)
- Isobe, A. (2020). Paleo-ocean de-stratification triggered by the subduction of the Oyashio water into the Sea of Japan after the Last Glacial Maximum. *Paleoceanography and Paleoclimatology*, 35(3), e2019PA003593. <https://doi.org/10.1029/2019PA003593>
- Itaki, T., Ikehara, K., Motoyama, I., & Hasegawa, S. (2004). Abrupt ventilation changes in the Japan Sea over the last 30 ky: Evidence from deep-dwelling radiolarians. *Palaeogeography, Palaeoclimatology, Palaeoecology*, 208(3–4), 263–278. <https://doi.org/10.1016/j.palaeo.2004.03.010>
- Itaki, T., Komatsu, N., & Motoyama, I. (2007). Orbital- and millennial-scale changes of radiolarian assemblages during the last 220 kyrs in the Japan Sea. *Palaeogeography, Palaeoclimatology, Palaeoecology*, 247(1–2), 115–130. <https://doi.org/10.1016/j.palaeo.2006.11.025>
- Jordi, A., & Wang, D.-P. (2012). sbPOM: A parallel implementation of Princeton Ocean Model. *Environmental Modelling & Software*, 38, 59–61. <https://doi.org/10.1016/j.envsoft.2012.05.013>
- Keigwin, L. D., & Gorbarenko, S. A. (1992). Sea level, surface salinity of the Japan Sea, and the Younger Dryas event in the northwestern Pacific Ocean. *Quaternary Research*, 37(3), 346–360. [https://doi.org/10.1016/0033-5894\(92\)90072-Q](https://doi.org/10.1016/0033-5894(92)90072-Q)
- Kida, S., Qiu, B., Yang, J., & Lin, X. (2016). The annual cycle of the Japan Sea Throughflow. *Journal of Physical Oceanography*, 46(1), 23–39. <https://doi.org/10.1175/JPO-D-15-0075.1>
- Kim, D., Shin, H.-R., Kim, C.-H., & Hirose, N. (2020). Characteristics of the East Sea (Japan Sea) circulation depending on surface heat flux and its effect on branching of the Tsushima Warm Current. *Continental Shelf Research*, 192, 104025. <https://doi.org/10.1016/j.csr.2019.104025>
- Kim, M., Hwang, J., Kim, G., Na, T., Kim, T. H., & Hyun, J. H. (2022). Carbon cycling in the East Sea (Japan Sea): A review. *Frontiers in Marine Science*, 9, 938935. <https://doi.org/10.3389/fmars.2022.938935>
- Kim, S., Park, Y., Kim, Y. H., Seo, S., Jin, H., Pak, G., & Lee, H. J. (2021). Origin, variability, and pathways of East Sea Intermediate Water in a high-resolution ocean reanalysis. *Journal of Geophysical Research: Oceans*, 126(6), e2020JC017158. <https://doi.org/10.1029/2020JC017158>
- Koizumi, I., & Yamamoto, H. (2011). Oceanographic variations over the last 150,000 yr in the Japan Sea and synchronous Holocene with the Northern Hemisphere. *Journal of Asian Earth Sciences*, 40(6), 1203–1213. <https://doi.org/10.1016/j.jseas.2010.06.013>
- Lee, E., Kim, S., & Nam, S. (2008). Paleo-Tsushima Water and its effect on surface water properties in the East Sea during the Last Glacial Maximum: Revisited. *Quaternary International*, 176–177, 3–12. <https://doi.org/10.1016/j.quaint.2007.03.021>
- Lee, E., & Nam, S. (2004). Low sea surface salinity in the East Sea during the Last Glacial Maximum: Review on freshwater supply. *Geoscience Journal*, 8(1), 43–49. <https://doi.org/10.1007/BF02910277>
- Lee, K. E. (2007). Surface water changes recorded in late Quaternary marine sediments of the Ulleung Basin, East Sea (Japan Sea). *Palaeogeography, Palaeoclimatology, Palaeoecology*, 247(1–2), 18–31. <https://doi.org/10.1016/j.palaeo.2006.11.019>
- Lee, K. E., Bahk, J. J., & Choi, J. (2008). Alkenone temperature estimates for the East Sea during the last 190,000 years. *Organic Geochemistry*, 39(6), 741–753. <https://doi.org/10.1016/j.orggeochem.2008.02.003>
- Li, D., Chen, J., Ni, X., Wang, K., Zeng, D., Wang, B., et al. (2019). Hypoxic bottom waters as a carbon source to atmosphere during a typhoon passage over the East China Sea. *Geophysical Research Letters*, 46(20), 11329–11337. <https://doi.org/10.1029/2019GL083933>
- Li, L., Lin, P., Yu, Y., Wang, B., Zhou, T., Liu, L., et al. (2013). The flexible global ocean-atmosphere-land system model, grid-point version 2: FGOALS-g2. *Advances in Atmospheric Sciences*, 30(3), 543–560. <https://doi.org/10.1007/s00376-012-2140-6>
- Liu, Y., Chen, J., Chen, J., Xing, L., Zou, J., & Yao, Z. (2014). Variations of alkenone temperature in the Sea of Japan during the last 170 ka and its paleoceanographic implications. *Chinese Science Bulletin*, 59(33), 4498–4509. <https://doi.org/10.1007/s11434-014-0367-6>
- Matsui, H., Tada, R., & Oba, T. (1998). Low-salinity isolation event in the Japan Sea in response to eustatic sea-level drop during LGM: Reconstruction based on salinity-balance model. *Quaternary Research*, 37(3), 221–233. <https://doi.org/10.4116/jaqua.37.221>
- Minato, S., & Kimura, R. (1980). Volume transport of the western boundary current penetrating into a marginal sea. *Journal of the Oceanographical Society of Japan*, 36(4), 185–195. <https://doi.org/10.1007/BF02070331>
- Miyazawa, Y., Zhang, R., Guo, X., Tamura, H., Ambe, D., Lee, J. S., et al. (2009). Water mass variability in the western North Pacific detected in a 15-year eddy resolving ocean reanalysis. *Journal of Oceanography*, 65(6), 737–756. <https://doi.org/10.1007/s10872-009-0063-3>
- Nakagawa, T., Kitagawa, H., Yasuda, Y., Tarasov, P. E., Nishida, K., Gotanda, K., et al. (2003). Asynchronous climate changes in the North Atlantic and Japan during the Last Termination. *Science*, 299, 688–691. <https://doi.org/10.1126/science.1078235>
- Nishida, N., & Ikehara, K. (2013). Holocene evolution of depositional processes off southwest Japan: Response to the Tsushima Warm Current and sea-level rise. *Sedimentary Geology*, 290, 138–148. <https://doi.org/10.1016/j.sedgeo.2013.03.012>
- Oba, T., & Irino, T. (2012). Sea level at the Last Glacial Maximum, constrained by oxygen isotopic curves of planktonic foraminifera in the Japan Sea. *Journal of Quaternary Science*, 27, 941–947. <https://doi.org/10.1002/jqs.2585>
- Oba, T., Kato, M., Kitazato, H., Koizumi, I., Omura, A., Sakai, T., & Takayama, T. (1991). Paleoenvironmental changes in the Japan Sea during the last 85,000 years. *Paleoceanography*, 6(4), 499–518. <https://doi.org/10.1029/91PA00560>
- Oba, T., & Tanimura, Y. (2012). Surface environments in the Japan Sea around the Last Glacial Maximum. *The Journal of the Geological Society of Japan*, 118(6), 376–386. <https://doi.org/10.5575/geosoc.2012.0011>
- Ohshima, K. I. (1994). The flow system in the Japan Sea caused by a sea level difference through shallow straits. *Journal of Geophysical Research*, 99(C5), 9925. <https://doi.org/10.1029/94JC00170>
- Park, J., & Lim, B. (2018). A new perspective on origin of the East Sea Intermediate Water: Observations of Argo floats. *Progress in Oceanography*, 160, 213–224. <https://doi.org/10.1016/j.pocan.2017.10.015>
- Park, Y.-H., & Khim, B.-K. (2022). Development of the East Korea Warm Current in the Hupo Trough of the southwestern East Sea (Japan Sea) since the Last Glacial Maximum based on TEX86 and U 37 K ' paleothermometers. *Organic Geochemistry*, 170, 104446. <https://doi.org/10.1016/j.orggeochem.2022.104446>
- Ravelo, A. C., & Hillaire-Marcel, C. (2007). Chapter eighteen the use of oxygen and carbon isotopes of foraminifera in paleoceanography. In C. Hillaire-Marcel & A. De Vernal (Eds.), *Developments in marine geology* (pp. 735–764). Elsevier.
- Sagawa, T., Nagahashi, Y., Satoguchi, Y., Holbourn, A., Itaki, T., Gallagher, S. J., et al. (2018). Integrated tephrostratigraphy and stable isotope stratigraphy in the Japan Sea and East China Sea using IODP sites U1426, U1427, and U1429, expedition 346 Asian monsoon. *Progress in Earth and Planetary Science*, 5(1), 18. <https://doi.org/10.1186/s40645-018-0168-7>
- Saito, Y., Katayama, H., Ikehara, K., Kato, Y., Matsumoto, E., Oguri, K., et al. (1998). Transgressive and highstand systems tracts and post-glacial transgression, the East China Sea. *Sedimentary Geology*, 122(1–4), 217–232. [https://doi.org/10.1016/S0037-0738\(98\)00107-9](https://doi.org/10.1016/S0037-0738(98)00107-9)

- Senjyu, T. (2022). Changes in mid-depth water mass ventilation in the Japan Sea deduced from long-term spatiotemporal variations of warming trends. *Frontiers in Marine Science*, 8, 766042. <https://doi.org/10.3389/fmars.2021.766042>
- Sherriff-Tadano, S., Abe-Ouchi, A., & Oka, A. (2021). Impact of mid-glacial ice sheets on deep ocean circulation and global climate. *Climate of the Past*, 17(1), 95–110. <https://doi.org/10.5194/cp-17-95-2021>
- Shin, H.-R., Lee, J.-H., Kim, C.-H., Yoon, J. H., Hirose, N., Takikawa, T., & Cho, K. (2022). Long-term variation in volume transport of the Tsushima Warm Current estimated from ADCP current measurement and sea level differences in the Korea/Tsushima Strait. *Journal of Marine Systems*, 232, 103750. <https://doi.org/10.1016/j.jmarsys.2022.103750>
- Spötl, C., Koltai, G., Jarosch, A. H., & Cheng, H. (2021). Increased autumn and winter precipitation during the Last Glacial Maximum in the European Alps. *Nature Communications*, 12(1), 1839. <https://doi.org/10.1038/s41467-021-22090-7>
- Stiller, J., Fonseca, R. R., Alfaro, M. E., Faircloth, B. C., Wilson, N. G., & Rouse, G. W. (2021). Using ultraconserved elements to track the influence of sea-level change on leafy seadragon populations. *Molecular Ecology*, 30(6), 1364–1380. <https://doi.org/10.1111/mec.15744>
- Tada, R. (1999). Late quaternary paleoceanography of the Japan Sea. *Quaternary Research*, 38(3), 216–222. <https://doi.org/10.4116/jaqua.38.216>
- Tada, R., Irino, T., Ikehara, K., Karasuda, A., Sugisaki, S., Xuan, C., et al. (2018). High-resolution and high-precision correlation of dark and light layers in the Quaternary hemipelagic sediments of the Japan Sea recovered during IODP Expedition 346. *Progress in Earth and Planetary Science*, 5(1), 19. <https://doi.org/10.1186/s40645-018-0167-8>
- Takikawa, T., Yoon, J.-H., & Cho, K.-D. (2005). The Tsushima Warm Current through Tsushima Straits estimated from ferryboat ADCP data. *Journal of Physical Oceanography*, 35(6), 1154–1168. <https://doi.org/10.1175/JPO2742.1>
- Teague, W. J., Jacobs, G. A., Perkins, H. T., Book, J. W., Chang, K. I., & Suk, M. S. (2002). Low-frequency current observations in the Korea/Tsushima Strait. *Journal of Physical Oceanography*, 32(6), 21–1641. [https://doi.org/10.1175/1520-0485\(2002\)032<1621:lfcot>2.0.co;2](https://doi.org/10.1175/1520-0485(2002)032<1621:lfcot>2.0.co;2)
- Topper, R. P. M., Flecker, R., Meijer, P. T., & Wortel, M. J. R. (2011). A box model of the Late Miocene Mediterranean Sea: Implications from combined ⁸⁷Sr/⁸⁶Sr and salinity data. *Paleoceanography*, 26(3), PA3223. <https://doi.org/10.1029/2010PA002063>
- Tsujino, H., Nakano, H., & Motoi, T. (2008). Mechanism of currents through the straits of the Japan Sea: Mean state and seasonal variation. *Journal of Oceanography*, 64(1), 141–161. <https://doi.org/10.1007/s10872-008-0011-7>
- Voltaire, A., Sanchez-Gomez, E., Salas y Mélia, D., Decharme, B., Cassou, C., Senesi, S., et al. (2013). The CNRM-CM5.1 global climate model: Description and basic evaluation. *Climate Dynamics*, 40(9–10), 2091–2121. <https://doi.org/10.1007/s00382-011-1259-y>
- Watanabe, S., Hajima, T., Sudo, K., Nagashima, T., Takemura, T., Okajima, H., et al. (2011). MIROC-ESM 2010: Model description and basic results of CMIP5-20c3m experiments. *Geoscientific Model Development*, 4, 845–872. <https://doi.org/10.5194/gmd-4-845-2011>
- Watanabe, S., Tada, R., Ikehara, K., Fujine, K., & Kido, Y. (2007). Sediment fabrics, oxygenation history, and circulation modes of Japan Sea during the Late Quaternary. *Paleoceanography, Palaeoclimatology, Palaeoecology*, 247(1–2), 50–64. <https://doi.org/10.1016/j.palaeo.2006.11.021>
- Wu, Y., Shi, X., Gong, X., Jian, Z., Zou, J., Liu, Y., et al. (2020). Evolution of the upper ocean stratification in the Japan Sea since the last glacial. *Geophysical Research Letters*, 47(16), e2020GL088255. <https://doi.org/10.1029/2020GL088255>
- Yanagi, T. (2002). Water, salt, phosphorus and nitrogen budgets of the Japan Sea. *Journal of Oceanography*, 58(6), 797–804. <https://doi.org/10.1023/A:1022815027968>
- Yang, H., Guo, X., Miyazawa, Y., Varlamov, S. M., Abe-Ouchi, A., & Chan, W. (2022). Changes in the Kuroshio path, surface velocity and transport during the last 35,000 years. *Geophysical Research Letters*, 49(4), e2021GL097250. <https://doi.org/10.1029/2021GL097250>
- Yang, J., & Pratt, L. J. (2013). On the effective capacity of the dense-water reservoir for the Nordic Seas overflow: Some effects of topography and wind stress. *Journal of Physical Oceanography*, 43(2), 418–431. <https://doi.org/10.1175/JPO-D-12-087.1>
- Yokoyama, Y., Esat, T. M., Thompson, W. G., Thomas, A. L., Webster, J. M., Miyairi, Y., et al. (2018). Rapid glaciation and a two-step sea level plunge into the Last Glacial Maximum. *Nature*, 559(7715), 603–607. <https://doi.org/10.1038/s41586-018-0335-4>
- Yokoyama, Y., Kido, Y., Tada, R., Minami, I., Finkel, R. C., & Matsuzaki, H. (2007). Japan Sea oxygen isotope stratigraphy and global sea-level changes for the last 50,000 years recorded in sediment cores from the Okai Ridge. *Paleoceanography, Palaeoclimatology, Palaeoecology*, 247(1–2), 5–17. <https://doi.org/10.1016/j.palaeo.2006.11.018>
- Yokoyama, Y., Lambeck, K., De Deckker, P., Johnston, P., & Fifield, L. K. (2000). Timing of the Last Glacial Maximum from observed sea-level minima. *Nature*, 406(6797), 713–716. <https://doi.org/10.1038/35021035>
- Yokoyama, Y., & Purcell, A. (2021). On the geophysical processes impacting palaeo-sea-level observations. *Geoscience Letters*, 8(1), 13. <https://doi.org/10.1186/s40562-021-00184-w>
- Yokoyama, Y., Purcell, A., & Ishiwa, T. (2019). Gauging quaternary sea level changes through scientific ocean drilling. *Oceanography*, 32(1), 64–71. <https://doi.org/10.5670/oceanog.2019.121>
- Yukimoto, S., Adachi, Y., Hosaka, M., Sakami, T., Yoshimura, H., Hirabara, M., et al. (2012). A new global climate model of the Meteorological Research Institute: MRI-CGCM3—Model description and basic performance. *Journal of the Meteorological Society of Japan Series II*, 90A, 23–64. <https://doi.org/10.2151/jmsj.2012-A02>
- Zheng, J., Guo, X., Yang, H., Du, K., Mao, X., Jiang, W., et al. (2022). Low sea surface salinity event of the Japan Sea during the Last Glacial Maximum [Dataset]. Zenodo. <http://doi.org/10.5281/zenodo.7146734>
- Zou, J., Shi, X., Liu, Y., Liu, J., Selvaraj, K., & Kao, S. J. (2012). Reconstruction of environmental changes using a multi-proxy approach in the Ulleung Basin (Sea of Japan) over the last 48 ka. *Journal of Quaternary Science*, 27(9), 891–900. <https://doi.org/10.1002/jqs.2578>